Biogeosciences Discuss., 10, 14539–14593, 2013
www.biogeosciences-discuss.net/10/14539/2013/
doi:10.5194/bgd-10-14539-2013

Biogeosciences Discussions
Open Access

An improved ocean model of aluminium: the effects of circulation, sediment resuspension and biological incorporation

M. M. P. van Hulten[1], A. Sterl[1], R. Middag[2,3,4], H. J. W. de Baar[4,5], M. Gehlen[6], J.-C. Dutay[6], and A. Tagliabue[7]

[1]Royal Netherlands Meteorological Institute (KNMI), Utrechtseweg 297, 3731 GA De Bilt, the Netherlands
[2]University of Otago, 364 Leith Walk, Dunedin, 9016, New Zealand
[3]University of California Santa Cruz (UCSC), 1156 High Street, Santa Cruz, CA 95064, USA
[4]Royal Netherlands Institute for Sea Research (NIOZ), Landsdiep 4, 1797 SZ 't Horntje, Texel, the Netherlands
[5]University of Groningen (RUG), Postbus 72, 9700 AB Groningen, the Netherlands
[6]Laboratoire des Sciences du Climat et de l'Environnement (LSCE), LSCE-Orme, point courrier 129, CEA-Orme des Merisiers, 91191 Gif-sur-Yvette Cedex, France
[7]University of Liverpool, 4 Brownlow Street, Liverpool L69 3GP, UK

Received: 12 July 2013 – Accepted: 21 July 2013 – Published: 2 September 2013

Correspondence to: M. M. P. van Hulten (marco@hulten.org)

Published by Copernicus Publications on behalf of the European Geosciences Union.

BGD
10, 14539–14593, 2013

Abstract

The distribution of dissolved aluminium (Al) in the ocean is of interest because of its potential impact on diatom remineralisation and the use of surface ocean Al as a tracer for dust. Previously, the ocean Al concentration has been simulated reasonably well with only a dust source and scavenging as the removal process. In this study the simulation has been significantly improved by a more refined circulation and the addition of a sediment resuspension source. The latter confirms that the most significant sources of Al to the ocean are dust deposition and sediment resuspension. Simulations with biological incorporation have been performed as well. These show that this can be an important removal process. However, this study does not provide a definitive answer to the question what the relative amount of incorporation is compared to scavenging.

1 Introduction

The cycling and distribution of aluminium in the ocean has received attention for several reasons, among which are the interactions between the cycles of aluminium (Al) and silicon (Si). Dissolved Al is scavenged by adsorption onto biogenic debris that settles as aggregates into the deep ocean, henceforth called Al_{ads}. In addition, dissolved Al becomes incorporated into biological opal ($SiO_2 \cdot nH_2O$), primarily the frustules of diatoms. The Al incorporated in opal of living diatoms is hereafter called Al_{diat}. The relatively heavy opal (density twice seawater) serves as ballast for settling aggregates, thus removing the adsorbed as well as the incorporated Al efficiently. This is consistent with the reduced levels of dissolved Al, associated with high diatom production. Conversely, the rate of dissolution of settling opal debris (hereafter called biogenic silica, Si_{biog}) appears to be controlled by the Al / Si element ratio in the opal debris. The higher the Al / Si ratio, the lower the rate of dissolution of the Si_{biog}.

Another major reason of the importance of Al is the use of Al as a tracer of aeolian dust supply into the surface ocean, which is an important source of the micronutrient

BGD
10, 14539–14593, 2013

iron. Indeed, it is currently assumed that the major source of Al to the open ocean is dust deposition (e.g. Kramer et al., 2004; Measures et al., 2005; de Jong et al., 2007; Middag et al., 2013b). A fraction of the Al in dust (1–15 %) dissolves within the upper mixed layer (Orians and Bruland, 1986; Maring and Duce, 1987; Jickells et al., 2005; Baker et al., 2006; Buck et al., 2006; Measures et al., 2010; Han et al., 2012), while below the mixed layer, the dissolution of Al from dust is deemed negligible (van Hulten et al., 2012). Most Al of dust (i.e. 85–99 %) remains in the particulate phase and sinks to the bottom of the ocean. This major portion that does not dissolve is assumed to be buried in the sediment.

The second source of Al is hypothesised to be sediment resuspension and subsequent dissolution, e.g. by desorption, of previously sedimented Al (Moran and Moore, 1991; Middag et al., 2012, 2013b). Indeed, a high concentration of dissolved aluminium (Al_{diss}) has been measured near the sediment in the West Atlantic Ocean at 45–50° N (Fig. 1a). One prerequisite is sufficient turbulence near the sediment. This is the case at several locations in the West Atlantic Ocean. Especially north of ∼ 40° N and south of ∼ 40° S, significant resuspension of sediment occurs (Biscaye and Eittreim, 1977; Gross et al., 1988). Another obvious prerequisite is an adequate supply of sedimenting Al towards the seafloor. Even though lithogenic particulate Al from dust deposition is such a supply, Al in that form is relatively refractory (Brown and Bruland, 2009). Hence, sedimenting Al associated with Si_{biog} is a more obvious candidate for redissolution. The scavenger and incorporator of Al, biogenic silica, is mostly present at regions underlying active diatom production (north of 40° N and south of 40° S, Nelson et al., 1995; Tréguer and De La Rocha, 2013), hence there this prerequisite is satisfied.

Nevertheless, not all sediments are a significant source of Al. Apparently, in the Southern Hemisphere, the desorption and dissolution of Al_{ads} from resuspended sediment is very small (Moran et al., 1992; Middag et al., 2011b). Upon settling on the seafloor, the desorption of adsorbed aluminium is controlled by the concentration of dissolved silicon in ambient seawater. At a higher dissolved Si concentration, the des-

BGD
10, 14539–14593, 2013

orption of Al is reduced (Mackin and Aller, 1986). Especially in the AntArctic Bottom Water (AABW) [Si_{diss}] is very high, preventing desorption of Al.

Other sources do not appear to play a significant role in adding Al to the ocean. Even though rivers carry a large concentration of Al, most of it is removed in estuaries and continental shelf sediments and never enters the open ocean (Mackin, 1986; Orians and Bruland, 1986; Brown et al., 2010; Jones et al., 2012). Finally, hydrothermal vents are not a source of Al to the deep waters of the oceans either (Hydes et al., 1986; Lunel et al., 1990; Elderfield and Schultz, 1996; Middag et al., 2011a).

The primary removal mechanism of Al_{diss} from the surface ocean is the adsorptive scavenging and settling with Si_{biog} as the major carrier, hence this removal is large in areas with high diatom production (Stoffyn and Mackenzie, 1982; Orians and Bruland, 1986; Moran and Moore, 1988, 1989; Bruland and Lohan, 2006). Besides being scavenged by surface adsorption, the Al_{diss} becomes incorporated as an apparent trace substitute for Si during growth of living diatoms. Following diatom mortality, the incorporated Al is exported with the Si_{biog} debris, i.e. becomes defined as the Al_{biog} pool (Stoffyn, 1979; Moran and Moore, 1988; Hydes et al., 1988; van Beusekom and Weber, 1992; Chou and Wollast, 1997; Gehlen et al., 2002; Middag et al., 2009). These processes are schematically presented in Fig. 2.

Incorporated Al is likely to inhibit the dissolution of Si_{biog} (Lewin, 1961; van Bennekom et al., 1991; van Beusekom and Weber, 1992; Dixit et al., 2001). This means that at a high Al_{diat}/Si_{diat} in living diatoms and consequent same ratio Al_{biog}/Si_{biog} in biogenic debris, there will be less Si_{biog} remineralised. Furthermore, more silica will be buried and hence lost from the system. Eventually less Si_{diss} will be returned to the surface through upwelling, resulting in decreased diatom production. This highlights the major link between Al and Si.

Recent years have seen the development of models of the marine biogeochemical cycle of aluminium. Gehlen et al. (2003) and van Hulten et al. (2012) implemented a scavenging model, while Han et al. (2008) also included biological incorporation of Al into the frustules of diatoms.

BGD
10, 14539–14593, 2013

Gehlen et al. (2003) had the objective of testing the sensitivity of modelled Al fields to dust input and thus to evaluate the possibility of constraining dust deposition via dissolved surface Al. For this purpose they embedded an Al cycle in the HAMOCC2 biogeochemical model (Maier-Reimer, 1993). The Al model consists of a reversible first-order relation of adsorption of Al_{diss} onto Si_{biog}. In chemical equilibrium the Al_{ads} concentration is proportional to the product of the concentrations of Al_{diss} and suspended particulate Si_{biog}. The resulting modelled concentration of Al_{diss} was of the same order as the then published observations. The model of van Hulten et al. (2012) used the same chemical equilibrium relation between adsorbed and dissolved Al. Instead of testing the effect of different dust fields, they tested the sensitivity to the solubility of Al from dust in the ocean surface and in the water column. This constrained the percentage and depth of dissolution of Al from the dust. The coefficient partitioning Al_{ads} and Al_{diss} was constrained as well with the respective sensitivity experiment. A sensitivity experiment with a margin sediment source showed that margin sediments are probably not an important source of Al. Deep ocean sediments are more likely to be important. The main goal of Han et al. (2008) was to better constrain the dust deposition field. For this purpose they used the Biogeochemical Elemental Cycling (BEC) model improved by Moore and Braucher (2008) as a starting point. This was used in combination with the model Dust Entrainment And Deposition (DEAD) to explicitly constrain dust deposition. In addition to scavenging, Han et al. (2008) added a biological Al uptake module where the Al : Si uptake ratio is a function of the ambient dissolved Al and Si concentrations. They did not expand on the importance of biological incorporation relative to scavenging.

These recently developed models have confirmed the first principles of Al cycling in the ocean, showing that the dissolution of Al from dust and the reversible scavenging by Si_{biog} can reproduce the main features of the observed Al_{diss} concentration. However, the deep ocean has not been simulated very well, and accurate deep ocean measurements of $[Al_{diss}]$ have only become available recently. These recent high accuracy observations from the West Atlantic Ocean Geotraces section show a mirror image

BGD
10, 14539–14593, 2013

between [Al_{diss}] and [Si_{diss}] (Fig. 1). This suggests, on the one hand that there is a very modest sediment source of Al into the ocean where [Si_{diss}] is relatively high, where the AABW prevails flowing from Antarctica up to 45° N. On the other hand, the Denmark Strait Overflow Water (DSOW) brings bottom waters with low [Si_{diss}] from the Denmark Strait (~ 66° N) to at least 45° N. This, in combination with ample supply of adsorbed Al from opal debris of diatom blooms in overlying surface waters, yields major desorption of Al from resuspended particles in the bottom waters in the 45–50° N region. Part of the desorbed Al will advect and mix into surrounding waters.

The other process of interest is that of biological incorporation of Al by diatoms. The goal in this research is to assess this as a significant process to explain the nutrient-like profiles of Al found in some regions of the ocean (Chou and Wollast, 1997; Middag et al., 2009). A simulation with incorporation is expected to yield a decrease of [Al_{diss}] compared to the simulation without incorporation. The decrease may even result in an unrealistically low [Al_{diss}] since scavenging parameters were tuned in the reference experiment to fit the open ocean main thermocline distribution of Al_{diss} and most of the West Atlantic Geotraces section at full depth.

In this study the model of van Hulten et al. (2012) is extended with three major changes. The different simulations address the role of circulation, the importance of a sediment source and the significance of biological incorporation of Al by diatoms. Details on this model and of the observational dataset are given in Sect. 2. Next, the results of the reference simulation and the three sensitivity experiments, relative to the reference simulation and to the simulation in van Hulten et al. (2012), are discussed in Sect. 3. Finally, Sect. 4 gives the major conclusions.

BGD
10, 14539–14593, 2013

2 Methods

2.1 Model description

2.1.1 Model framework

In order to model the three-dimensional distribution of dissolved Al, the biogeochemical model PISCES has been used (Aumont and Bopp, 2006; Ethé et al., 2006). This model has been employed for many other studies concerning trace metals, as well as large scale ocean biogeochemistry (e.g. Aumont and Bopp, 2006; Gehlen et al., 2007; Arsouze et al., 2009; Dutay et al., 2009; Tagliabue et al., 2010). In the simulations described here, PISCES has been driven by climatological velocity fields obtained from the general circulation model called *Nucleus for European Modelling of the Ocean* (NEMO) (Madec, 2008) of which the dynamical component is called OPA (Madec et al., 1998).

The model PISCES simulates the cycle of carbon, the major nutrients (nitrate, phosphate, ammonium, silicic acid) and the trace nutrient iron, along with two phytoplankton types (nanophytoplankton and diatoms), two zooplankton grazers (micro- and mesozooplankton), two classes of particulate organic carbon (small and large) of differential settling speeds, as well as calcite and biogenic silica. The PISCES model distinguishes three silicon pools: the silicon content of living diatoms (Si_{diat}); the silicon content of dead, settling diatoms (Si_{biog}) and dissolved silicic acid (Si_{diss}). In the model, Si_{diss} and other nutrients are supplied to the ocean by means of atmospheric dust deposition and rivers, while iron enters the ocean as well through sediment remobilisation (Aumont and Bopp, 2006). The standard version of PISCES accounts for 24 tracers. For a more detailed description of PISCES see the auxiliary material of Aumont and Bopp (2006).

BGD
10, 14539–14593, 2013

2.1.2 Aluminium model

The Al model is based on (van Hulten et al., 2012, henceforth vH12) which computes the concentration of dissolved aluminium (Al_{diss}) and adsorbed Al (Al_{ads}). In this study two additional tracers are introduced to PISCES: the Al incorporated in the opaline frustules of living diatoms (Al_{diat}) and its biogenic debris (Al_{biog}). The concentrations of these tracers, usually indicated by square brackets [] are, for the sake of clarity, denoted without the brackets in the model equations below. There are two different sources of Al in the model. One source is via the dissolution of dust particles at the ocean surface. The dust deposition field was taken from the output of the atmospheric dust model INCA (Hauglustaine et al., 2004; Textor et al., 2006). The other source is sediment resuspension and subsequent dissolution, that has now been added to the previous model. When the Al_{ads} reaches the ocean floor, it is assumed to be buried, except for the resuspension and subsequent dissolution of Al in some simulations. The model is schematically represented in Fig. 2, where the extensions to vH12 (black) are shown in red and green.

The model parameters are listed in Table 1. The aluminium fraction in dust (f_{Al}) is based on the mass percentages of Al known to be present in the Earth's crust. This is about 8.1 % aluminium on average (Wedepohl, 1995). Most of this Al consists of oxides that do not dissolve easily. The fraction of Al from dust (α) that dissolves is not well constrained but is probably in the range of 1–15 % (Orians and Bruland, 1986; Measures and Vink, 2000; Jickells et al., 2005) and $\alpha = 5\,\%$ is a working modelling value (Han et al., 2008; van Hulten et al., 2012). The dissolution occurs only in the upper model layer (0–10 m depth range), and is described by the following equation:

$$\left.\frac{\partial Al_{diss}}{\partial t}\right|_{deposition} = \frac{\alpha \cdot f_{Al}}{m_{Al} \cdot \Delta z_1} \cdot \Phi_{dust}\,, \tag{1}$$

where m_{Al} is the atomic mass of Al, $\Delta z_1 = 10\,m$ is the thickness of the surface model layer and Φ_{dust} is the dust flux into the ocean. The Al that does not dissolve from dust is

BGD
10, 14539–14593, 2013

assumed to play no role in the biogeochemical cycle of Al on our timescales of interest, and can be thought of as being buried in marine sediments.

Another source of Al is sediment resuspension (red arrow in Fig. 2). In reality, this is induced by near-sediment turbulence, creating a layer of water above the sediment containing significant amounts of suspended sediment particles. This layer is about 200 to 1000 m thick and is referred to as the *nepheloid layer* (Jackson, 2005). Due to the low vertical resolution of the model (bottom layer is up to 500 m thick), it is not attempted to parameterise sediment resuspension by means of the turbulence parameters present in the model. Instead, a certain portion of settled biogenic silica is redissolved into the bottom model layer. This portion depends on several conditions, among which the amount of dissolvable Al particles. There are no observations or good estimates of Al flux from sediment resuspension, while there is also no sediment model of Al available. Therefore it is assumed that recently settled Al_{ads} is resuspended and subsequently partially dissolved (e.g. Lampitt, 1985). Since the resuspension depends on settling of Al_{ads}, the relevant model equation will be introduced at the end of this section, after the settling equation.

Dissolved Al is assumed to adsorb onto biogenic silica particles and, aside from external inputs (and optionally the incorporation within the silica), the Al_{diss} concentration is governed by adsorption and desorption (black horizontal arrows in Fig. 2). The Al_{diss} and Al_{ads} concentrations follow the following reversible first-order adsorption equation (vH12):

$$\left.\frac{\partial Al_{ads}}{\partial t}\right|_{ad/desorption} = \kappa(Al_{ads}^{eq} - Al_{ads}) \,, \tag{2}$$

where

$$Al_{ads}^{eq} = k_d \cdot Al_{diss} \cdot Si_{biog} \,, \tag{3}$$

in which Al_{ads}^{eq} is the chemical equilibrium concentration of Al_{ads}. The parameter k_d is the partition coefficient and κ is the first order rate constant for equilibration of Al_{ads} to

BGD
10, 14539–14593, 2013

Al^{eq}_{ads}. Since total Al is conserved when only internal processes are concerned, the time derivative of Al_{diss} equals the negative of that of Al_{ads}.

As an extension to the original model, aluminium is incorporated into the frustules of diatoms during production. The diatom incorporation of Al is modelled by multiplying the rate of production of diatom opal (Si_{diat}) with the Al / Si concentration ratio in ambient seawater, with some refinements as explained below. For the biological Si cycle, production and mortality (including grazing by micro- and mesozooplankton) of diatoms, and dissolution of debris Si_{biog}, are represented by prod, mort and diss, respectively. These Si rate variables are multiplied by the Al / Si element ratio in the respective pools to arrive at the corresponding Al rate variables. In other words, all rate variables are proportional to the ratio of Al and Si in the relevant source pool. Accordingly, the biological model equations for Al are as follows:

$$\left.\frac{\partial Al_{diat}}{\partial t}\right|_{bio} = \xi \cdot prod - \frac{Al_{diat}}{Si_{diat}} \cdot mort \tag{4a}$$

$$\left.\frac{\partial Al_{biog}}{\partial t}\right|_{bio} = \frac{Al_{diat}}{Si_{diat}} \cdot mort - \frac{Al_{biog}}{Si_{biog}} \cdot diss \tag{4b}$$

$$\left.\frac{\partial Al_{diss}}{\partial t}\right|_{bio} = \frac{Al_{biog}}{Si_{biog}} \cdot diss - \xi \cdot prod\,. \tag{4c}$$

No further refinement is made in any process, except, optionally, for incorporation during production, using the optional term ξ, which is defined as:

$$\xi = \min\left(k_{in} \cdot \frac{Al_{diss}}{Si_{diss}},\, r_{max}\right)\,, \tag{5}$$

with k_{in} ($0 \le k_{in} \lesssim 1$) a weight factor for the Al : Si incorporation ratio, and r_{max} is a prescribed maximum value for the Al_{diat} / Si_{diat} ratio within the opal of living diatoms. This refinement is not used in the model simulations presented in this work (i.e. $k_{in} = 1$ and $r_{max} = \infty$), but will be discussed in Sect. 3.4 on biological incorporation.

BGD
10, 14539–14593, 2013

Both Al_{biog} and Al_{ads} settle downwards through the water column because the associated biogenic silica is denser than seawater. Adsorbed and incorporated Al (both denoted as Al_{part}) settle along with biogenic silica with a speed w_s, varying from 30 m d^{-1} in the upper 100 m, to 200 m d^{-1} at 4 km below the mixed layer, according to

$$\left.\frac{\partial Al_{part}}{\partial t}\right|_{sinking} = -\frac{\partial}{\partial z}(w_s \cdot Al_{part}) \,. \quad (6)$$

While settling through the water column, Al_{biog} and Al_{ads} may remineralise (Eqs. 4b and 2, respectively), so adsorption and incorporation do not mean that all Al is removed immediately from the model domain. Part of the Al dissolves and may upwell and may become incorporated or scavenged once again at a later time.

Burial proceeds in the bottom model layer immediately above the sediment according to $\partial Al_{part} / \partial t = -(w_s \cdot Al_{part}) / \Delta z_{bottom}$, where $\Delta z_{bottom} \leq 500$ m is the thickness of the bottom layer and is of the same order as the real resuspension layer, or nepheloid layer. In some of the simulations, part of the sedimented Al_{ads} is resuspended and dissolved in the bottom water layer according to:

$$\left.\frac{\partial Al_{diss}}{\partial t}\right|_{resusp} = \beta \cdot \frac{w_s \cdot Al_{ads}}{\Delta z_{bottom}} \,, \quad (7)$$

where β is a constant ($0 < \beta \leq 1$) or some scalar function to be defined later (Eq. 8), representing the fraction of resuspended and subsequently dissolved Al. The underlying rationale and the derivation of Eq. (7) is given in the Appendix. Moreover, silicic acid near the sediment apparently inhibits the dissolution of Al_{ads}. This is probably because Al_{diss} and Si_{diss} are stoichiometrically saturated (Mackin and Aller, 1986). Observations suggest a significant Al sediment source below Denmark Strait Overflow Water (DSOW) where Si_{diss} concentrations are below 30 µM (1 µM = 10^{-6} mol dm^{-3}), while they suggest only a very weak source from the sediment below AABW, which has much higher [Si_{diss}], exceeding 50 µM (Middag et al., 2013b). In the simulations,

BGD
10, 14539–14593, 2013

the bottom water [Si_{diss}] will be used as an inhibitor of the redissolution of Al from resuspended sediment.

In this study the PISCES model is run off-line forced by a climatological year of monthly physical fields including turbulent diffusion. All model fields are defined on the ORCA2 grid, an irregular grid covering the whole world ocean with a nominal resolution of $2^{\circ} \times 2^{\circ}$, with the meridional resolution increased near the equator. It has two "north poles" in Canada and Russia to eliminate the coordinate singularity in the Arctic Ocean. Its vertical resolution is 10 m in the upper 100 m, increasing downwards to 500 m, such that there are 30 layers in total and the ocean has a maximum depth of 5000 m.

The source code of the model is included as an electronic supplement. This code can be used with NEMO-PISCES version 3.1, to be found at http://www.nemo-ocean.eu/ (libre software licensed under CeCILL).

2.1.3 Simulations

The reference simulation is based on the reference simulation from vH12, but there is one notable improvement. A different set of dynamical fields (advection, turbulent diffusion and mixing) is now used. The velocity fields used by vH12 had an Atlantic Meridional Overturning Circulation (MOC) that is too shallow and too weak, while AABW was too strong. The fields used in this study are a climatology from a NEMO-OPA run forced by DFS3 air–sea fluxes (Brodeau et al., 2010). These dynamics have a more realistic Atlantic overturning, compared to those used by vH12. Firstly, the depth of North Atlantic Deep Water is about 2 km in vH12 while it is closer to the more reasonable 3 km in the dynamics used here. Secondly, the maximum of the Atlantic Overturning Stream Function (OSF) in the AABW dropped from about 6–7 Sv in the old dynamics to about 2–3 Sv in the new dynamics, much more comparable to estimates based on observations (Talley et al., 2003). This results in a significantly better simulation of the Si_{diss} distribution. The Si_{diss} concentration in AABW is much closer to the observational concentration, compared with the dynamical fields used by vH12 (basic statistics for the West Atlantic Ocean are presented in Sect. 3.2). This will especially be important for

BGD
10, 14539–14593, 2013

one of the sediment resuspension simulations described below, since that simulation depends on [Si_{diss}] in bottom water.

The reference experiment is initialised from vH12 and is then run for another 1250 model years to steady state. From years 650 and 1000 this simulation is forked to several sensitivity simulations to run another 250 yr alongside the reference experiment. An overview of all key parameters for the simulations is given in Table 2.

For all experiments, the same dust dissolution and scavenging parameters are used as by vH12 (see Table 1), resulting in a good simulation of [Al_{diss}] in the main thermocline. The sensitivities of the model to most of these parameters were tested by vH12. There is no sediment source or biological incorporation of Al in the base experiment.

In the first of our two sediment resuspension simulations, 60 % of sedimented Al_{ads} is redissolved just above the sediment. This means that β from Eq. (7) is a constant ($\beta = 0.60$). However, the West Atlantic Ocean Geotraces observations show a large elevation of [Al_{diss}] due to resuspension only in the Northern Hemisphere and only very little, if at all, in the Southern Hemisphere (Fig. 1a). We reckon this elevation of [Al_{diss}] in bottom waters is due to significant dissolution/desorption from resuspended sediment in part of the Northern Hemisphere, a process apparently inhibited in the Southern Hemisphere. The explanation here is by the mirror image distribution of dissolved silicate (Fig. 1b) that is very high in the AABW in the Southern Hemisphere and flows as far north as $\sim 40^{\circ}$ N, albeit somewhat diluted by vertical mixing with overlying NADW that has lower Si_{diss} concentrations. High concentration of Si_{diss} in bottom waters apparently prevents the dissolution/desorption of Al from sediments. Briefly, in the northernmost part of the section the DSOW cascades down over the seafloor from $\sim 65^{\circ}$ N to $\sim 45^{\circ}$ N underway acquiring more and more dissolved Al due to redissolution/desorption from resuspended sediment particles in the here very intense bottom nepheloid layer (Biscaye and Eittreim, 1977; Gross et al., 1988). Indeed from 65° N to 45° N the dissolved Al in the deepest bottom water sample increases linearly ($p < 0.001$ and $r^2 = 0.96$ for $n = 10$) with decreasing latitude from 12 nM at 65° N to 34 nM at 44.8° N (Middag et al., 2013b, their Supplement Fig. S3). The parallel increase

BGD
10, 14539–14593, 2013

of $[Si_{diss}]$ is relatively modest from 8 µM at 65° N to 21 µM at 44.8° N. However, somewhere in between 45° N and 40° N the southward flowing DSOW becomes underlain by the northward extreme of AABW with much higher $[Si_{diss}] \approx 45$ µM at 39.5° N that appears to inhibit any further dissolution/desorption of Al from suspended sediments.

The overall sediment source of Al_{diss} is likely due to a combination of processes (bottom current velocity, resuspension, partial dissolution of clay minerals, partial dissolution of biogenic debris (Si_{biog}, Al_{biog}) and desorption) where pore water chemistry within the sediments likely plays a role as well. However, neither the actual observations (Fig. 1a) of dissolved Al nor the simulation modelling have the adequate vertical resolution to resolve all these processes. Instead for the simulation, by following Mackin and Aller (1986) and the derivation in the Appendix, we simulate that a fraction β of only the Al_{ads} will dissolve again by desorption (above Eq. 7) where β depends on $[Si_{diss}]$ in the bottom water as follows:

$$\beta = 16.85 \cdot ([Si_{diss}]_{bottom}/\mu M)^{-0.828}\,, \tag{8}$$

where admittedly the "critical value" (here defined as $[Si_{diss}]$ where 50 % of sedimenting Al_{ads} redissolves in the bottom water) for largely preventing desorption/dissolution of Al is set at somewhat higher ~ 70 µM than the above mentioned apparent threshold of ~ 45 µM. Nevertheless, redissolution of Al is small when bottom water $[Si_{diss}]$ is high, and vice versa. If the apparent observed threshold were to be used, too much Al would redissolve in AABW.

Finally, the simulation with biological incorporation of Al into diatom frustules is performed without any limitation to the incorporation of Al_{diss}. This means that for this simulation, $k_{in} = 1$ and $r_{max} = \infty$ (see Eq. 5), or that $\xi = Al_{diss}/Si_{diss}$; alternatives will be discussed in Sect. 3.

2.2 Observational datasets

Recent Geotraces observations of $[Al_{diss}]$ in the Arctic Ocean (Middag et al., 2009), North-east Atlantic Ocean (Middag, 2010, chap. 5), West Atlantic Ocean (Middag et al.,

BGD
10, 14539–14593, 2013

2013b), the Atlantic sector of the Southern Ocean (Middag et al., 2011b, 2012, 2013a) and the region south of Australia (Remenyi, 2013) are used for a detailed comparison and optimisation of the model parameters. See the upper part of Table 3 for these datasets and Fig. 3 for the station positions. These datasets comprise overall 3893 individual data values for dissolved Al. All values have been verified versus international reference samples and their consensus values of the SAFe and Geotraces programmes. See vH12 for more details. In contrast to vH12, the Geotraces International Polar Year (GIPY) data by (Remenyi, 2013, data and dissertation on request available from lead author) have been added to the dataset, namely SAZ-Sense (GIPY2) and SR3 (GIPY6). Those are 438 extra data points compared to the number used by vH12.

For a worldwide global ocean comparison one also has to rely on data that was collected in the era before the reference samples of SAFe and Geotraces were available. Inevitably, the definition of criteria for selecting such previously published datasets is less strict, see vH12 and (Middag, 2010, 216–218) for the criteria used for each of the selected datasets. The selected datasets are listed in the lower part of Table 3 and station positions are shown in Fig. 3.

2.3 Data–model comparison

For the visual comparison between model and observations, horizontal and vertical cross sections of the model data are plotted. With the same colour scale observations are plotted as coloured dots to directly compare the model with the observations.

For the horizontal [Al_{diss}] sections four different depths are presented, where "surface" signifies the average over the upper 30 m, "500 m" is 450–550 m averaged, "2500 m" is 2450–2550 m averaged and "4500 m" is 4450–4550 m averaged. The respective observations (same depth ranges) are presented as coloured dots. The colour scale is not linear to better show the main features at both low and high concentrations of Al_{diss}.

The vertical [Al_{diss}] sections are of the Geotraces sections in the West Atlantic Ocean (64 PE *n* and JC057 from Table 3) and the Zero Meridian Southern Ocean (part of

BGD
10, 14539–14593, 2013

ANT XXIV/3). These sections are calculated from the three-dimensional model data by converting the ORCA2 gridded model data to a rectilinear mapping and interpolating the rectilinear data onto the cruise track coordinates. Those figures also show the Atlantic Overturning Stream Function (OSF), defined as the zonally (through the Atlantic Ocean) and vertically (from the surface downward) integrated meridional current speed. This is used as a measure for the Meridional Overturning Circulation (MOC).

The focus of this study is the West Atlantic Ocean for several reasons. Firstly, recently measurements have been done in that region (Geotraces), resulting in a large consistent (one method) dataset. Secondly, there are too few high-quality observations in other regions of the ocean, making it very difficult to define a reasonable goodness of fit. Thirdly, the West Atlantic Ocean is of large importance to the MOC and hence the deep ocen cycling of nutrients. For these reasons all quantitative arguments in this study concern the West Atlantic Geotraces section.

2.3.1 Statistics

To compare the model results with the observations of the West Atlantic Ocean Geotraces section (Sect. 3), first the observations are linearly interpolated onto the model grid. Then several statistics are determined, namely the Root Mean Square Deviation (RMSD), the Reliability Index RI and the correlation coefficient r. They are all based on Stow et al. (2009), but the first two are adjusted for the inhomogeneous sample distribution in depth.

The RMSD is determined by the following equation:

$$\mathrm{RMSD}_{\updownarrow} = \sqrt{\frac{\sum_{k=1}^{30} \Delta z_k \cdot \sum_{j=1}^{60} (m_{jk} - o_{jk})^2}{60 \cdot \sum_{k=1}^{30} \Delta z_k}}, \tag{9}$$

where o is the observed and m the modelled [$\mathrm{Al}_{\mathrm{diss}}$], weighing with model layer thickness Δz_k of layer $k \in \{1 \ldots 30\}$ for every station $j \in \{1 \ldots 60\}$. The $\updownarrow$ signifies the vertical

BGD
10, 14539–14593, 2013

weighing modification to the standard RMSD by Stow et al. (2009). This is done to compensate for the overrepresentation of data points near the ocean surface. Furthermore, the significance of the RMSD differences is calculated. This is determined by means of a Monte Carlo simulation on the reference experiment for which a subsample of 400 has been randomly selected from the original set of 1650 data-model points. These are the pairs of observations and model data, both on the model grid. This is done 50 000 times and from this the 2σ confidence interval is calculated (the mean ± two times the standard deviation). For each experiment y comparing with an experiment x, the average RMSD of the Monte Carlo simulation of y should be outside the 2σ confidence range of the RMSD distribution of x to say that y is a significant improvement or worsening of x.

The reliability index adjusted by weighing with the model layer thickness is defined as:

$$\mathrm{RI}_{\updownarrow} = \exp\sqrt{\frac{\sum_{k=1}^{30}\Delta z_k \sum_{j=1}^{60}\left(\log\frac{o_{jk}}{m_{jk}}\right)^2}{60\cdot\sum_{k=1}^{30}\Delta z_k}}. \quad (10)$$

Finally, the correlation coefficient is defined as:

$$r = \frac{\sum_{i=1}^{1800}(o_i-\overline{o})(m_i-\overline{m})}{\sqrt{\sum_{i=1}^{1800}(o_i-\overline{o})^2\sum_{i=1}^{1800}(m_i-\overline{m})^2}}, \quad (11)$$

where 1800 is the total number of measurements of the West Atlantic Geotraces section and the bars denote averages.

BGD
10, 14539–14593, 2013

3 Results and discussion

3.1 Reference simulation and observations

Our reference experiment has been performed for a spin-up period of 1250 yr, starting from vH12, with improved dynamics. The resulting total Al budget (both dissolved and adsorbed) in the world ocean in the reference simulation is around 6 Tmol (1 Tmol = 10^{12} mol). After 650 yr of simulation the total Al distribution does not change much (Fig. 4). Therefore, from 650 yr our sensitivity experiments with biological incorporation are forked and run for at least 200 yr. Simulations where deep ocean circulation might play an important role (sediment resuspension), are forked from 1000 yr.[1]

Figure 5 shows the modelled Al_{diss} concentration of the reference experiment at four depths versus observations as coloured dots, and in Fig. 6 the Geotraces sections in the West Atlantic Ocean and the Zero Meridian Southern Ocean are presented. In the surface the highest modelled and observed [Al_{diss}] is located in the Atlantic Ocean from near the equator northwards to about 35° N. In the polar oceans and the South Pacific Ocean, the [Al_{diss}] is very low. In the West Atlantic section, the MOC is clearly reflected by the dissolved Al concentration. The decrease of [Al_{diss}] from north to south in the North Atlantic Deep Water (NADW) is due to net adsorptive scavenging onto biogenic silica.

The similarity between the model and the observations decreases in the deeper North Atlantic Ocean, where according to the observations [Al_{diss}] increases with depth (for depths below 800 m), while in the model the dissolved Al concentration decreases with depth. Besides this general pattern of increase of [Al_{diss}] with depth in the observations, a very high concentration of Al_{diss} is present between 45 and 50° N near the sediment, which enhances the dissimilarity between the model and the observations.

[1]The relevant tracers of the raw model output can be found at http://data.zkonet.nl/index.php?page=Project_view&id=2916&tab=Datasets.

BGD
10, 14539–14593, 2013

3.2 Improved dynamics

In this dynamical forcing the maximum southward transport is at a reasonably realistic depth of almost 3 km (contour in Fig. 6), while vH12 used a forcing with the maximum Atlantic OSF closer to 2 km. The more reasonable OSF depth results in a better simulation of $[Al_{diss}]$ in the West Atlantic Ocean (Fig. 6). The $RMSD_{\updownarrow}$ of $[Al_{diss}]$ of the reference simulation from vH12 versus observations is 8.24 nM, while the $RMSD_{\updownarrow}$ of this new simulation versus observations is 7.65 nM. This is an improvement albeit the difference between these RMSD values is still insignificant (Table 4).

The first two rows in Table 4 present the goodness of fit statistics for $[Si_{diss}]$. Inspecting the $RMSD_{\updownarrow}$, the reference experiment with the dynamics used in this paper is a significant improvement to the ones used in vH12. Since $[Si_{diss}]$ improves, it is likely that the Si cycle as a whole is improved, but an assessment of the Si cycle is beyond the scope of this paper. However, the improved Si_{diss} distribution gives credibility to the $[Si_{diss}]$-dependent sediment resuspension simulation. If the modelled $[Si_{diss}]$ were very different from the observed $[Si_{diss}]$, such a simulation would be less trustworthy.

3.3 Sediment resuspension

Van Hulten et al. (2012) performed a sediment input simulation. However, that experiment was modelled analogous to iron (Fe). Typically in shallow waters, Fe diffuses from the sediment into the water above by build-up of reduced Fe. There is no such effect known for Al. The sediment input experiment in this work is based on sediment resuspension in deep ocean bottom waters and has the biggest effect where sedimentation of Al_{ads} is highest and bottom water $[Si_{diss}]$ is sufficiently low.

Figure 7 shows $[Al_{diss}]$ resulting from the simulation in which sediment resuspension is proportional only to $w_s Al_{part}$ at the bottom ($\beta = 0.60$). In the Northern Hemisphere, the deep $[Al_{diss}]$ is simulated much better in this experiment than in the original one (Fig. 6), but in the Southern Hemisphere $[Al_{diss}]$ is simulated much worse. The dissolved Al concentration is much too high near the bottom, and elevated $[Al_{diss}]$ levels are found

BGD
10, 14539–14593, 2013

throughout the whole water column. Nonetheless, the addition of resuspension in this way does significantly improve the simulation ($RMSD_{\updownarrow}$ = 5.06 nM, compared to 7.65 nM for the reference simulation). However, in the southern Atlantic Ocean and along the Zero Meridian in the Southern Ocean, sediment input should be much closer to zero.

When the [Si_{diss}]-dependent parameterisation based on Mackin and Aller (1986) is used (β according to Eq. 8), the spatial comparison between the observations and the model becomes much better. Figure 8a shows [Al_{diss}] from this bottom [Si_{diss}]-dependent sediment resuspension experiment. As expected, also in this experiment the sediment resuspension source of Al results in a higher [Al_{diss}] near 40–60° N in the deep North Atlantic Ocean (Fig. 8b) compared to the reference simulation. Furthermore, there are several characteristics that this simulation reproduces better than the sediment resuspension simulation that is independent of bottom [Si_{diss}]. Firstly, [Al_{diss}] is only slightly larger near the sediment in the Southern Hemisphere compared to the overlying water (Fig. 8b). The observations extend to practically the bottom of the ocean (almost 6000 m at some latitudes of the Geotraces West Atlantic section), while the model depth is only 5000 m. This makes a good comparison of deep ocean [Al_{diss}] between model and observations difficult, but the slightly elevated [Al_{diss}] in the near-sediment observations is consistent with the slight elevation in the bottom model layer. Secondly, the region from 0° to 45° N at a depth below 2 km has a higher [Al_{diss}] compared to the reference simulation (Fig. 6) and better represents the observations. Based on the low [Si_{diss}] alone, a high near-sediment [Al_{diss}] is expected north of 55° N as well, but this is not found. Most Al_{diss} in the surface waters in the North Atlantic Drift is scavenged before reaching 55° N. Therefore the supply of Al from surface waters to the seafloor is very limited. Hence there is only a small amount of redissolution of sedimented Al north of 55° N, consistent with the observations. As expected, the resuspended Al_{diss} mixes into the NADW, but most of it is scavenged again before reaching 40° S, just like the reversibly scavenged Al from the dust deposition. The overall resulting [Al_{diss}] is more consistent with the observations compared to the original simulation without any sediment resuspension ($RMSD_{\updownarrow}$ = 4.71 nM). The difference with the origi-

BGD
10, 14539–14593, 2013

nal simulation ($RMSD_{\updownarrow}$ = (7.65±0.81) nM) is a statistically significant improvement (see Table 4).

Figure 9 shows [Al_{diss}] at four depths for the simulation with sediment resuspension (parametrisation based on Mackin and Aller, 1986), with observations as coloured dots. Figure 10 shows the difference of [Al_{diss}] between this simulation the reference simulation. In several semi-enclosed basins, like the Gulf of Mexico and the Arctic Ocean, and the Atlantic Ocean, [Al_{diss}] is higher compared to the reference simulation, especially near the sediment. The Gulf of Mexico, the Mediterranean Sea, Baffin Bay and the Arctic Ocean may contribute to Atlantic Ocean [Al_{diss}]. However, the increase of near-sediment [Al_{diss}] in the West Atlantic Ocean at 45–50° N is much more likely caused by in situ resuspension and subsequent dissolution (Fig. 8b).

The $RMSD_{\updownarrow}$ between this experiment (sediment resuspension depending on bottom [Si_{diss}]) and the observations is significantly lower than from the reference experiment (Table 4). This, together with the presented concentration plots, shows that the sediment redissolution process is an improvement of the model. This supports the hypothesis of a sediment source of Al in the form of resuspension and subsequent dissolution in the real ocean.

In none of the simulations the modelled [Al_{diss}] is higher than 35.4 nM while observations go up to 48.6 nM. The reason might be that scavenging is too strong. Decreasing k_d may remedy this problem. However, some of the data points that are already overestimated most extremely in the model, would also get higher. The results of the combined biological incorporation and decreased k_d simulation at the end of the paper present further material for discussion on this issue. The combination of overestimated low concentrations (all depths) and underestimated high concentrations (especially deep ocean) suggests that the model needs more fundamental changes than a simple tuning of parameters.

BGD
10, 14539–14593, 2013

3.4 Biological incorporation

The relative difference between the simulated [Al_{diss}] with biological incorporation and without is presented in Fig. 11 at four depths. In the main thermocline, north of 60° S, [Al_{diss}] is significantly lower (Fig. 11a and b), while in the deep ocean at low latitudes (in the eastern Atlantic and northern Indian Ocean) it is slightly elevated compared to the reference simulation (Fig. 11d). While the reference experiment simulates the observed [Al_{diss}] well in the upper part of the ocean, in this new simulation too much Al is removed from the upper part of the ocean.

The significantly lower [Al_{diss}] in the main thermocline in this simulation, compared with the reference simulation, makes the modelled concentrations much lower than the observed concentrations. This does not mean that biological incorporation of Al by diatoms does not occur. It only implies that this way of incorporating Al into the frustules in this model with its current configuration yields an unrealistically low value of [Al_{diss}]. There are several ways to compensate this effect so that future simulations may still be able to support the incorporation hypothesis.

Firstly, too much Al might be incorporated into the living diatoms. A different moderation term ξ would be able to change that. One way is to set k_{in} very low as is done by Han et al. (2008). They defined $k_{in} = 0.08845$, loosely based on Gehlen et al. (2002). Alternatively, one may also define a maximum incorporation of $r_{max} = 0.007$, based on the same paper, or 0.0022, an incorporation ratio based on observations of [Al_{diss}] and [Si_{diss}] at remineralisation depth (Middag et al., 2009), or as high as 0.03 (Van Beusekom, personal communication, January 2013). Simulations were performed with the parameterisation by Han et al. (2008), i.e. with $k_{in} = 0.08845$ and $r_{max} = \infty$ (results not presented here). These simulations do not yield significant changes compared to the reference experiment. Hence, from these simulations it cannot be concluded whether incorporation (with a reduced incorporation rate k_{in}) occurs.

Secondly, whether incorporation is moderated or not, the model is likely to need retuning, since incorporation functions as an extra sink of Al. The sedimentation speed

BGD
10, 14539–14593, 2013

w_s and scavenging parameters κ and k_d may need to be adjusted (see Eqs. 2, 3 and 6). For instance, the partition coefficient k_d may be decreased. This leaves more Al_{diss} in the surface ocean, compensating the decrease of $[Al_{diss}]$ by incorporation. But this does not work. To show this, a simulation has been performed with incorporation and a decreased k_d. In Fig. 12 the relative concentration difference between this simulation and the reference simulation is presented. The decrease in the Atlantic Ocean surface is slightly smaller than in the case with incorporation and a high k_d (compare with Fig. 11). However, in the Southern Ocean $[Al_{diss}]$ has increased by a considerable amount, yielding concentrations much higher than the observed concentrations. This is because in the model, scavenging and incorporation are fundamentally different from each other. On the one hand, adsorbed Al, in equilibrium given by Eq. (3), is proportional to both $[Al_{diss}]$ and $[Si_{biog}]$. On the other hand, incorporation, as given by Eq. (4a), is only proportional to $[Al_{diss}]$ (and the growth of diatoms, $\partial Si_{diat}/\partial t$) and not proportional to $[Si_{biog}]$. Furthermore, Si_{biog} is present below the photic zone as well, resulting in scavenging throughout a significant amount of the water column. Incorporation, on the other hand, only occurs in the photic zone. Hence, decreasing k_d not only affects the photic zone, where an increase of $[Al_{diss}]$ is needed to compensate for incorporation, but also the aphotic zone. Biogenic Si strongly depends on latitude, with the polar oceans having high $[Si_{biog}]$. On the one hand, incorporation of Al mostly occurs in the Atlantic Ocean (because of high dust deposition). On the other hand, scavenging is especially strong in the polar oceans. Because of high $[Si_{biog}]$ at those regions, k_d has a much stronger sensitivity in the polar oceans compared to other locations (vH12). A smaller k_d therefore results in more Al_{diss} in the Southern Ocean, while it has little effect on the more problematic incorporation-induced decrease of $[Al_{diss}]$ in the Atlantic Ocean. The $RMSD_{\updownarrow}$ between this simulation and the observations (at the West Atlantic Geotraces section) is 8.68 nM. Even though this is a significant improvement compared with the incorporation simulation with original scavenging, it is still a significant worsening compared with the reference simulation. Decreasing the first-order rate constant κ

BGD
10, 14539–14593, 2013

has a very similar effect as decreasing k_d: it does not solve the problem in the Atlantic Ocean, while $[Al_{diss}]$ in the Southern Ocean increases too much (results not presented).

Increasing dust deposition is another possibility to compensate the decrease of $[Al_{diss}]$ in the main thermocline. A preliminary simulation suggests that more dust only significantly affects the very surface of the ocean. Dust deposition does not affect the subsurface $[Al_{diss}]$ much (at 50–400 m depth), while as a consequence of biological incorporation a strong depletion of Al_{diss} occurs there as well (result not presented here). Dissolving Al from dust below the ocean surface is an option. This has been done in vH12 by means of instantaneous dissolution upon deposition according to a function that is exponentially decreasing with depth. Dust deposition is rather localised. The depth-dependent dissolution function can be fitted to the observations or the reference simulation, giving a reasonable first-order simulation of $[Al_{diss}]$. Obviously, a simulation with a dissolution function fitted to the observations is not very strong evidence for incorporation.

From these considerations, it may be concluded, within the limitations of the model, that if incorporation is an important process at all, it is unlikely to occur proportional to the ambient Al_{diss} / Si_{diss} ratio.

4 Conclusions

The Al_{diss} distribution in the upper part of the ocean has been simulated reasonably well with only a dust source and reversible scavenging as the removal process (vH12). However, $[Al_{diss}]$ was strongly underestimated in the deep North Atlantic Ocean. The simulation is significantly improved by the use of different dynamical fields and the addition of a resuspension source. The latter supports the idea that the most significant sources of Al to the ocean are dust deposition and sediment resuspension, and the most important internal process could be adsorptive scavenging. Sediment resuspension depends on both Al_{ads} sedimentation and bottom water $[Si_{diss}]$. It has been shown

BGD
10, 14539–14593, 2013

that a parameterisation based on Mackin and Aller (1986) is able to simulate the deep ocean [Al_{diss}], supporting the idea of stoichiometric saturation.

The used dataset of measurements of [Al_{diss}] in the deep and bottom waters is much larger than hitherto available. Nevertheless, the vertical resolution when approaching the deep ocean seafloor still is modest. Similarly, the deepest bottom water box of the model extends to 500 m above the seafloor, and in some regions the model extent of 5000 m is less than the true full water column depth. Obviously, the very intriguing sediment source of Al in the 40 to 65° N region would be of great interest for a more detailed study with high vertical resolution sampling just above the seafloor and similar high vertical resolution modelling.

Experiments with biological incorporation have been performed as well. They show that biological incorporation of Al is unlikely to occur proportional to the ambient Al_{diss} / Si_{diss} ratio. The simulations suggest that the relative importance of incorporation compared to scavenging may be small, because changing the scavenging parameters or surface dust dissolution cannot compensate for the unrealistic simulated decrease of dissolved Al in the main thermocline. This does not imply that incorporation does not take place, yet perhaps net incorporation is relatively small. It also needs to be realised that not all possibly relevant variables of the model have been tested extensively. This is largely due to the large expense of computer simulation time for each simulation run. Clearly, more simulations, laboratory experiments and field observations are needed to answer what the relative amount of incorporation is compared to scavenging.

Appendix A

Sediment resuspension model

Based on observations, Mackin and Aller (1986) hypothesised that Al redissolution is inhibited by pore water silicic acid ($Si(OH)_4$). They wrote the following, using () for chemical activity and p for $-\log_{10}$ as also in pH:

BGD
10, 14539–14593, 2013

In general, when stoichiometric saturation (sensu Thorstenson and Plummer, 1977) exists for an authigenic clay of constant composition in sediment pore waters having nearly invariant reactive cation concentrations, the following will hold (Mackin and Aller, 1984).

$$p(\mathrm{Al(OH)_4^-}) + ap(\mathrm{Si(OH)_4}) + b\,\mathrm{pH} = pK_{\mathrm{eq}}\,, \tag{A1}$$

where [$a = \mathrm{Si}/\mathrm{Al}$ and $b = \mathrm{H^+}/\mathrm{Al}$ are the stoichiometries] of the clay and pK_{eq} = apparent constant excluding the effects of major cations and other potentially reactive cations. To estimate values of a and b for the Amazon shelf sediments from [their] Fig. 2, we applied a regression technique which treats $p(\mathrm{Al(OH)_4^-})$, $p(\mathrm{Si(OH)_4})$ and pH as independent variables (Mackin and Aller, 1984). The results of this treatment give the following:

$$1(\pm 0.044)p(\mathrm{Al(OH)_4^-}) + 0.828(\pm 0.093)p(\mathrm{Si(OH)_4}) + 0.429(\pm 0.070)\mathrm{pH} = pK_{\mathrm{eq}}\,, \tag{A2}$$

where $pK_{\mathrm{eq}} = 13.98(\pm 0.13)$.

The chemical activities are in nM and µM for $\mathrm{Al(OH)_4^-}$ and $\mathrm{Si(OH)_4}$, respectively. Their use of stoichiometric saturation is consistent with the mirror image between $[\mathrm{Al(OH)_4^-}]$ and $[\mathrm{Si(OH)_4}]$ as shown in Fig. 1b. Here $[\mathrm{Al(OH)_4^-}]_{\mathrm{bottom}}$ is small in the Southern Hemisphere and large in the Northern Hemisphere, while both south of 40° S and north of 40° N sediment particles are present in the bottom water (Fig. A1), strongly suggesting sediment resuspension.

Eq. (A1) can be rewritten to ($\mathrm{Al_{diss}} = \mathrm{Al(OH)_4^-}$, $\mathrm{Si_{diss}} = \mathrm{Si(OH)_4}$):

$$\log_{10}(\mathrm{Al_{diss}})_{\mathrm{pore}} + a \cdot \log_{10}(\mathrm{Si_{diss}})_{\mathrm{pore}} = B\,, \tag{A3}$$

with $B = b\mathrm{pH} - pK_{\mathrm{eq}}$ being an approximate constant (for pH = 8.1, $B = -10.5$). The dissolved entities between the brackets are *chemical activities* in the *pore water*, but

BGD
10, 14539–14593, 2013

we need to model *fluxes* from *resuspended sediment* into *bottom water*. We will refer to the model layer (of max. 500 m thick) just above the sediment as *bottom water*.

Since (Al_{diss}) and (Si_{diss}) are high in pore water (at least (Si_{diss}) is very high in Southern Ocean pore water), the chemical activities are not equal to the concentrations, but they are proportional to each other with the activity coefficients γ_{Al} and γ_{Si} (e.g. Stone and Morgan, 1990):

$$\begin{aligned} [Al_{diss}]_{pore} &= \gamma_{Al}(Al_{diss})_{pore} \\ [Si_{diss}]_{pore} &= \gamma_{Si}(Si_{diss})_{pore} \,. \end{aligned} \tag{A4}$$

So far we just rewrote the equations of Mackin and Aller (1986) using simple mathematics and chemistry. We will now introduce the model. For this purpose we will assume that the empirical relationship of Mackin and Aller (1986) (Eq. A1), found at the Amazon shelf, is valid everywhere. This assumption is defendable if Mackin and Aller (1986) have not made any extra implicit assumptions on top of the research of Thorstenson and Plummer (1977); the latter only used established thermodynamical relations.

From Eqs. (A3) and (A4) the following relation can be derived:

$$\begin{aligned} \log_{10}\frac{[Al_{diss}]_{pore}}{\gamma_{Al}} &= B - a\cdot\log_{10}\frac{[Si_{diss}]_{pore}}{\gamma_{Si}} \\ [Al_{diss}]_{pore}\,nM^{-1} &= \gamma_{Al}\cdot 10^{B}\cdot\left(\frac{[Si_{diss}]_{pore}}{\mu M\cdot\gamma_{Si}}\right)^{-a} \\ &= C\cdot([Si_{diss}]_{pore}\,\mu M^{-1})^{-a}\,, \end{aligned} \tag{A5}$$

where $C = 10^{B}\gamma_{Al}\gamma_{Si}^{a} \in \mathbb{R}^{+}$.

The Al flux Φ_{sed} from the bottom water layer to the sediment is given by $\Phi_{sed} = w_s\cdot[Al_{ads}]$, with $[Al_{ads}]$ the bottom water layer concentration of adsorbed Al and w_s the sedimentation rate. In line with the sediment resuspension hypothesis we assume the

BGD
10, 14539–14593, 2013

resuspended flux Φ_{resusp} to be proportional to Φ_{sed}, converting part of the sedimented Al into dissolved Al in the bottom water layer:

$$\Phi_{\text{resusp}} = \beta \cdot \Phi_{\text{sed}} = \beta \cdot w_s \cdot [\text{Al}_{\text{ads}}] \,, \tag{A6}$$

where $\beta \in [0,1]$ is the fraction of resuspended and subsequently dissolved Al. In the original resuspension model, β is a constant. In the more complex model, the resuspension flux is taken to be proportional to $[\text{Al}_{\text{diss}}]_{\text{pore}}$ (as well as $[\text{Al}_{\text{ads}}]$). Using Eq. (A5), this results in:

$$\beta \propto [\text{Al}_{\text{diss}}]_{\text{pore}}\,\text{nM}^{-1} \propto ([\text{Si}_{\text{diss}}]_{\text{pore}}\,\mu\text{M}^{-1})^{-a} \,. \tag{A7}$$

Furthermore, we assume that bottom water $[\text{Si}_{\text{diss}}]$ is proportional to pore water $[\text{Si}_{\text{diss}}]$. Together with Eqs. (A6) and (A7) this gives for the change of $[\text{Al}_{\text{diss}}]$ in the bottom layer due to resuspension:

$$\begin{aligned} \left.\frac{\partial[\text{Al}_{\text{diss}}]}{\partial t}\right|_{\text{resusp}} &= \frac{\Phi_{\text{resusp}}}{\Delta z_{\text{bottom}}} = \beta \cdot \frac{\Phi_{\text{sed}}}{\Delta z_{\text{bottom}}} \\ &= \beta_0 \left(\frac{[\text{Si}_{\text{diss}}]_{\text{bottom}}}{\mu\text{M}}\right)^{-a} \cdot \frac{\Phi_{\text{sed}}}{\Delta z_{\text{bottom}}} \,, \end{aligned} \tag{A8}$$

where β_0 is a dimensionless constant and Δz_{bottom} is the thickness of the bottom seawater model layer.

Since there can be no more redissolution than the amount of Al that sediments (assuming steady state and no horizontal remobilisation of sediment), β is at most one. If we want to use the highest possible flux for resuspension near 45–50° N, we set $\beta = 1$ in that region. The modelled bottom water $[\text{Si}_{\text{diss}}]$ near 50° N is 30.3 µM. Hence, the proportionality constant is $\beta_0 = 30.3^{0.828} = 16.85$. Since bottom $[\text{Si}_{\text{diss}}]$ farther north is lower, β would there be higher than one. Since the model assumes that only recently sedimented Al_{ads} is resuspended, it would not be physically correct if $\beta > 1$. Therefore

BGD
10, 14539–14593, 2013

β is constrained and hence given by:

$$\beta = \min(16.85 \cdot ([\mathrm{Si_{diss}}]\,\mu\mathrm{M}^{-1})^{-0.828}, 1)\,, \tag{A9}$$

which is to be plugged into the concentration change:

$$\left.\frac{\partial[\mathrm{Al_{diss}}]}{\partial t}\right|_{\mathrm{resusp}} = \beta \cdot \frac{\Phi_{\mathrm{sed}}}{\Delta z_{\mathrm{bottom}}}\,. \tag{A10}$$

This equation is identical to Eq. (7) in the main text, hence this result is what was to be demonstrated.

As a sanity check we substitute the minimum (13.4 µM) and the maximum (148.6 µM) bottom $[\mathrm{Si_{diss}}]$ into this equation:

$$\beta_{\mathrm{max}} = \min(16.85 \cdot 13.4^{-0.828}, 1) = \min(1.96, 1) = 1$$

$$\beta_{\mathrm{min}} = \min(16.85 \cdot 148.6^{-0.828}, 1) = 0.27$$

This means that since bottom $[\mathrm{Si_{diss}}]$ is decreasing with latitude, we expect 100 % re-dissolution anywhere north of 45° N (it is set up like that). About a quarter is dissolved in the Southern Ocean (high $[\mathrm{Si_{diss}}]$).

A sediment model is not present in the standard PISCES model. To work around this limitation, several assumptions needed to be made of which some may not be easy to defend. Alternatively, a sediment model may be coupled to PISCES. Implementing such a model needs further data and research concerning aluminosilicates in the deep benthic boundary layer and the top sediment.

Supplementary material related to this article is available online at: http://www.biogeosciences-discuss.net/10/14539/2013/bgd-10-14539-2013-supplement.zip.

BGD
10, 14539–14593, 2013

Acknowledgements. The authors are grateful to those who have been proved useful in discussion, among which Justus van Beusekom, Tom Remenyi, Micha Rijkenberg, Wilco Hazeleger and our colleagues from the IMAU institute. We also want to thank Christoph Heinze and Phoebe Lam for providing their data. The authors wish to acknowledge the use of the free software visualisation and analysis programs Ferret and R. Other noteworthy libre software used is the GNU Operating System and Climate Data Operators. Useful tips for statistical analysis were provided by Ronald van Haren, Carlo Lacagnina and Paul Hiemstra. This research is funded by the Netherlands Organisation for Scientific Research (NWO), grant Nr. 839.08.414, part of the ZKO programme.

References

Arsouze, T., Dutay, J.-C., Lacan, F., and Jeandel, C.: Reconstructing the Nd oceanic cycle using a coupled dynamical–biogeochemical model, Biogeosciences, 6, 2829–2846, doi:10.5194/bg-6-2829-2009, 2009. 14546

Aumont, O. and Bopp, L.: Globalizing results from ocean in situ iron fertilization studies, Global Biogeochem. Cy., 20, GB2017, doi:10.1029/2005GB002591, 2006. 14546

Baker, A., Jickells, T., Witt, M., and Linge, K.: Trends in the solubility of iron, aluminium, manganese and phosphorus in aerosol collected over the Atlantic Ocean, Mar. Chem., 98, 43–58, doi:10.1016/j.marchem.2005.06.004, 2006. 14542

Behrenfeld, M., O'Malley, R., Siegel, D., McClain, C., Sarmiento, J., Feldman, G., Milligan, A., Falkowski, P., Letelier, R., and Boss, E.: Climate-driven trends in contemporary ocean productivity, Nature, 444, 752–755, doi:10.1038/nature05317, 2006. 14593

Biscaye, P. and Eittreim, S.: Suspended particulate loads and transports in the nepheloid layer of the abyssal Atlantic Ocean, Mar. Geol., 23, 155–172, doi:10.1016/0025-3227(77)90087-1, 1977. 14542, 14552

Brodeau, L., Barnier, B., Treguier, A.-M., Penduff, T., and Gulev, S.: An ERA40-based atmospheric forcing for global ocean circulation models, Ocean Model., 31, 88–104, doi:10.1016/j.ocemod.2009.10.005, 2010. 14551

Brown, M. and Bruland, K.: Dissolved and particulate aluminum in the Columbia River and coastal waters of Oregon and Washington: behavior in near-field and far-field plumes, Estuar. Coast. Shelf S., 84, 171–185, doi:10.1016/j.ecss.2009.05.031, 2009. 14542

BGD
10, 14539–14593, 2013

Brown, M., Lippiatt, S., and Bruland, K.: Dissolved aluminum, particulate aluminum, and silicic acid in northern Gulf of Alaska coastal waters: glacial/riverine inputs and extreme reactivity, Mar. Chem., 122, 160–175, doi:10.1016/j.marchem.2010.04.002, 2010. 14543

Bruland, K. and Lohan, M.: Controls of trace metals in seawater, in: The Oceans and Marine Geochemistry, edited by: Elderfield, H., vol. 6, chap. 6.02, 23–47, Elsevier, available at: http://es.ucsc.edu/~kbruland/Manuscripts/BRULAND/BrulandChpt6_02_TraceMetals.pdf, 2006. 14543

Buck, C., Landing, W., Resing, J., and Lebon, G.: Aerosol iron and aluminum solubility in the northwest Pacific Ocean: results from the 2002 IOC cruise, Geochem. Geophy. Geosy., 7, Q04M07, doi:10.1029/2005GC000977, 2006. 14542

Chou, L. and Wollast, R.: Biogeochemical behavior and mass balance of dissolved aluminum in the western Mediterranean Sea, Deep-Sea Res. Pt. II, 44, 741–768, doi:10.1016/S0967-0645(96)00092-6, 1997. 14543, 14545

de Jong, J., Boyé, M., Gelado-Caballero, M., Timmermans, K., Veldhuis, M., Nolting, R., van den Berg, C., and de Baar, H.: Inputs of iron, manganese and aluminium to surface waters of the Northeast Atlantic Ocean and the European continental shelf, Mar. Chem., 107, 120–142, 2007. 14542

Dixit, S., Van Cappellen, P., and van Bennekom, A.: Processes controlling solubility of biogenic silica and pore water build-up of silicic acid in marine sediments, Mar. Chem., 73, 333–352, doi:10.1016/S0304-4203(00)00118-3, 2001. 14543

Dutay, J., Lacan, F., Roy-Barman, M., and Bopp, L.: Influence of particle size and type on ^{231}Pa and ^{230}Th simulation with a global coupled biogeochemical-ocean general circulation model: a first approach, Geochem. Geophy. Geosy., 10, Q01011, doi:10.1029/2008GC002291, 2009. 14546

Elderfield, H. and Schultz, A.: Mid-ocean ridge hydrothermal fluxes and the chemical composition of the ocean, Annu. Rev. Earth Pl. Sc., 24, 191–224, 1996. 14543

Ethé, C., Aumont, O., Foujols, M.-A., and Lévy, M.: NEMO reference manual, tracer component : NEMO-TOP, preliminary version, Note du Pole de Modélisation, Institut Pierre-Simon Laplace, 2006. 14546

Gehlen, M., Beck, L., Calas, G., Flank, A., van Bennekom, A., and van Beusekom, J.: Unraveling the atomic structure of biogenic silica: evidence of the structural association of Al and Si in diatom frustules, Geochim. Cosmochim. Ac., 66, 1601–1609, doi:10.1016/S0016-7037(01)00877-8, 2002. 14543, 14561

BGD
10, 14539–14593, 2013

Gehlen, M., Heinze, C., Maier-Reimer, E., and Measures, C.: Coupled Al–Si geochemistry in an ocean general circulation model: a tool for the validation of oceanic dust deposition fields?, Global Biogeochem. Cy., 17, 1028, doi:10.1029/2001GB001549, 2003. 14543

Gehlen, M., Gangstø, R., Schneider, B., Bopp, L., Aumont, O., and Ethe, C.: The fate of pelagic $CaCO_3$ production in a high CO_2 ocean: a model study, Biogeosciences, 4, 505–519, doi:10.5194/bg-4-505-2007, 2007. 14546

Gross, T. F., Williams, A., and Newell, A.: A deep-sea sediment transport storm, Nature, 331, 518–521, doi:10.1038/331518a0, 1988. 14542, 14552

Han, Q., Moore, J., Zender, C., and Hydes, D.: Constraining oceanic dust deposition using surface ocean dissolved Al, Global Biogeochem. Cy., 22, GB2038, doi:10.1029/2007GB002975, 2008. 14543, 14544, 14547, 14561

Han, Q., Zender, C. S., Moore, J. K., Buck, C. S., Chen, Y., Johansen, A., and Measures, C. I.: Global estimates of mineral dust aerosol iron and aluminum solubility that account for particle size using diffusion-controlled and surface-area-controlled approximations, Global Biogeochem. Cy., 26, GB2038, doi:10.1029/2011GB004186, 2012. 14542

Hauglustaine, D. A., Hourdin, F., Jourdain, L., Filiberti, M.-A., Walters, S., Lamarque, J.-F., and Holland, E. A.: Interactive chemistry in the Laboratoire de Météorologie Dynamique general circulation model: description and background tropospheric chemistry evaluation, J. Geophys. Res.-Atmos., 109, D04314, doi:10.1029/2003JD003957, 2004. 14547

Hydes, D., Statham, P., and Burton, J.: A vertical profile of dissolved trace metals (Al, Cd, Cu, Mn, Ni) over the median valley of the mid Atlantic ridge, 43° N: implications for hydrothermal activity, Sci. Total Environ., 49, 133–145, doi:10.1016/0048-9697(86)90236-6, 1986. 14543

Hydes, D., de Lange, G., and de Baar, H. J. W.: Dissolved aluminium in the Mediterranean, Geochim. Cosmochim. Ac., 52, 2107–2114, doi:10.1016/0016-7037(88)90190-1, 1988. 14543

Jackson, J.: Glossary of Geology, 5th revised and enlarged edn., Springer, Berlin, 2005. 14548

Jickells, T., An, Z., Andersen, K., Baker, A., Bergametti, G., Brooks, N., Cao, J., Boyd, P., Duce, R., Hunter, K. A., Kawahata, H., Kubilay, N., laRoche, J., Liss, P. S., Mahowald, N., Prospero, J. M., Ridgwell, A. J., Tegen, I., and Torres, R.: Global iron connections between desert dust, ocean biogeochemistry, and climate, Science, 308, 67–71, doi:10.1126/science.1105959, 2005. 14542, 14547

BGD
10, 14539–14593, 2013

Jones, M. T., Pearce, C. R., and Oelkers, E. H.: An experimental study of the interaction of basaltic riverine particulate material and seawater, Geochim. Cosmochim. Ac., 77, 108–120, doi:10.1016/j.gca.2011.10.044, 2012. 14543

Kramer, J., Laan, P., Sarthou, G., Timmermans, K., and De Baar, H.: Distribution of dissolved aluminium in the high atmospheric input region of the subtropical waters of the North Atlantic Ocean, Mar. Chem., 88, 85–101, doi:10.1016/j.marchem.2004.03.009, 2004. 14542, 14579

Kremling, K.: The distribution of cadmium, copper, nickel, manganese, and aluminium in surface waters of the open Atlantic and European shelf area, Deep-Sea Res., 32, 531–555, doi:10.1016/0198-0149(85)90043-3, 1985. 14579

Lampitt, R.: Evidence for the seasonal deposition of detritus to the deep-sea floor and its subsequent resuspension, Deep-Sea Res., 32, 885–897, doi:10.1016/0198-0149(85)90034-2, 1985. 14548

Lewin, J.: The dissolution of silica from diatom walls, Geochim. Cosmochim. Ac., 21, 182–198, doi:10.1016/S0016-7037(61)80054-9, 1961. 14543

Lunel, T., Rudnicki, M., Elderfield, H., and Hydes, D.: Aluminium as a depth-sensitive tracer of entrainment in submarine hydrothermal plumes, Nature, 344, 137–139, doi:10.1038/344137a0, 1990. 14543

Mackin, J.: Control of dissolved Al distributions in marine sediments by clay reconstitution reactions: experimental evidence leading to a unified theory, Geochim. Cosmochim. Ac., 50, 207–214, doi:10.1016/0016-7037(86)90170-5, 1986. 14543

Mackin, J. and Aller, R.: Dissolved Al in sediments and waters of the East China Sea: implications for authigenic mineral formation, Geochim. Cosmochim. Ac., 48, 281–297, doi:10.1016/0016-7037(84)90251-5, 1984. 14565

Mackin, J. and Aller, R.: The effects of clay mineral reactions on dissolved Al distributions in sediments and waters of the Amazon continental shelf, Cont. Shelf Res., 6, 245–262, doi:10.1016/0278-4343(86)90063-4, 1986. 14543, 14550, 14553, 14559, 14560, 14564, 14566

Madec, G.: NEMO ocean engine, Note du Pole de Modélisation, Institut Pierre-Simon Laplace, 2008. 14546

Madec, G., Delecluse, P., Imbard, M., and Lévy, C.: OPA 8.1 Ocean General Circulation Model reference manual, Note du Pole de Modélisation, Institut Pierre-Simon Laplace, 11, 91 pp., available at: http://hal.archives-ouvertes.fr/hal-00154217/en/, (last access: 2 September 2013), 1998. 14546

BGD
10, 14539–14593, 2013

Maier-Reimer, E.: Geochemical cycles in an ocean general circulation model: preindustrial tracer distributions, Global Biogeochem. Cy., 7, 645–677, doi:10.1029/93GB01355, 1993. 14544

Maring, H. and Duce, R.: The impact of atmospheric aerosols on trace metal chemistry in open ocean surface seawater, 1. Aluminum, Earth Planet. Sc. Lett., 84, 381–392, doi:10.1016/0012-821X(87)90003-3, 1987. 14542

Measures, C. and Vink, S.: On the use of dissolved aluminum in surface waters to estimate dust deposition to the ocean, Global Biogeochem. Cy., 14, 317–327, doi:10.1029/1999GB001188, 2000. 14547

Measures, C., Brown, M., and Vink, S.: Dust deposition to the surface waters of the western and central North Pacific inferred from surface water dissolved aluminum concentrations, Geochem. Geophy. Geosy., 6, Q09M03, doi:10.1029/2005GC000922, 2005. 14542

Measures, C., Sato, T., Vink, S., Howell, S., and Li, Y.: The fractional solubility of aluminium from mineral aerosols collected in Hawaii and implications for atmospheric deposition of biogeochemically important trace elements, Mar. Chem., 120, 144–153, doi:10.1016/j.marchem.2009.01.014, 2010. 14542

Middag, R.: Dissolved Aluminium and Manganese in the Polar Oceans, Ph.D. thesis, University of Groningen, Groningen, the Netherlands, 2010. 14553, 14554

Middag, R., de Baar, H., Laan, P., and Bakker, K.: Dissolved aluminium and the silicon cycle in the Arctic Ocean, Mar. Chem., 115, 176–195, doi:10.1016/j.marchem.2009.08.002, 2009. 14543, 14545, 14553, 14561, 14579

Middag, R., de Baar, H. J. W., Laan, P., Cai, P., and van Ooijen, J.: Dissolved manganese in the atlantic sector of the southern ocean, Deep-Sea Res. Pt. II, 58, 2661–2677, doi:10.1016/j.dsr2.2010.10.043, 2011a. 14543

Middag, R., van Slooten, C., de Baar, H. J. W., and Laan, P.: Dissolved aluminium in the Southern Ocean, Deep-Sea Res. Pt. II, 58, 2647–2660, doi:10.1016/j.dsr2.2011.03.001, 2011b. 14542, 14554, 14579

Middag, R., de Baar, H., Laan, P., and Huhn, O.: The effects of continental margins and water mass circulation on the distribution of dissolved aluminum and manganese in Drake Passage, J. Geophys. Res., 117, C01019, doi:10.1029/2011JC007434, 2012. 14542, 14554

Middag, R., de Baar, H., Klunder, M., and Laan, P.: Fluxes of dissolved aluminum and manganese to the Weddell Sea and indications for manganese co-limitation, Limnol. Oceanogr., 58, 287–300, doi:10.4319/lo.2013.58.1.0287, 2013a. 14554

BGD
10, 14539–14593, 2013

Middag, R., van Aken, H., van Hulten, M., and de Baar, H.: Aluminium in the ocean: unique mirror image of the biological cycle, in preparation, 2013b. 14542, 14550, 14552, 14553, 14579, 14581
Moore, J. K. and Braucher, O.: Sedimentary and mineral dust sources of dissolved iron to the world ocean, Biogeosciences, 5, 631–656, doi:10.5194/bg-5-631-2008, 2008. 14544
Moran, S. B. and Moore, R. M.: Temporal variations in dissolved and particulate aluminum during a spring bloom, Estuar. Coast. Shelf S., 27, 205–215, doi:10.1016/0272-7714(88)90090-X, 1988. 14543
Moran, S. B. and Moore, R. M.: The distribution of colloidal aluminum and organic carbon in coastal and open ocean waters off Nova Scotia, Geochim. Cosmochim. Ac., 53, 2519–2527, doi:10.1016/0016-7037(89)90125-7, 1989. 14543
Moran, S. B. and Moore, R. M.: The potential source of dissolved aluminum from resuspended sediments to the North Atlantic Deep Water, Geochim. Cosmochim. Ac., 55, 2745–2751, doi:10.1016/0016-7037(91)90441-7, 1991. 14542
Moran, S. B., Moore, R. M., and Westerlund, S.: Dissolved aluminum in the Weddell Sea, Deep-Sea Res., 39, 537–547, doi:10.1016/0198-0149(92)90087-A, 1992. 14542
Nelson, D., Tréguer, P., Brzezinski, M., Leynaert, A., and Quéguiner, B.: Production and dissolution of biogenic silica in the ocean: revised global estimates, comparison with regional data and relationship to biogenic sedimentation, Global Biogeochem. Cy., 9, 359–359, 1995. 14542
Obata, H., Alibo, D., and Nozaki, Y.: Dissolved aluminum, indium, and cerium in the Sea of Japan and the Sea of Okhotsk: comparison to the marginal seas of the western North Pacific, J. Geophys. Res., 112, C12003, doi:10.1029/2006JC003944, 2007. 14579
Orians, K. and Bruland, K.: The biogeochemistry of aluminum in the Pacific Ocean, Earth Planet. Sci. Lett., 78, 397–410, doi:10.1016/0012-821X(86)90006-3, 1986. 14542, 14543, 14547, 14579
Remenyi, T.: Investigating the impact of aeolian deposition to the Southern Ocean using dissolved aluminium concentrations, Doctor of philosophy in quantitative marine science, Quantitative Marine Science Program, UTas and CSIRO joint program, 2013. 14554, 14579
Slemons, L., Murray, J., Resing, J., Paul, B., and Dutrieux, P.: Western Pacific coastal sources of iron, manganese, and aluminum to the Equatorial Undercurrent, Global Biogeochem. Cy., 24, GB3024, doi:10.1029/2009GB003693, 2010. 14579

BGD
10, 14539–14593, 2013

Stoffyn, M.: Biological control of dissolved aluminum in seawater: experimental evidence, Science, 203, 651, doi:10.1126/science.203.4381.651, 1979. 14543
Stoffyn, M. and Mackenzie, F.: Fate of dissolved aluminum in the oceans, Mar. Chem., 11, 105–127, doi:10.1016/0304-4203(82)90036-6, 1982. 14543
Stone, A. and Morgan, J.: Kinetics of chemical transformation in the environment, in: Aquatic Chemical Kinetics: Reaction Rates of Processes in Natural Waters, edited by: Stumm, W., vol. 2, chap. 1, 1–42, John Wiley and Sons, 1990. 14566
Stow, C., Jolliff, J., McGillicuddy Jr., D. J., Doney, S. C., Allen, J. I., Friedrichs, M. A. M., Rose, K. A., and Wallhead, P.: Skill assessment for coupled biological/physical models of marine systems, J. Marine Syst., 76, 4–15, doi:10.1016/j.jmarsys.2008.03.011, 2009. 14555, 14556
Tagliabue, A., Bopp, L., Dutay, J.-C., Bowie, A. R., Chever, F., Jean-Baptiste, P., Bucciarelli, E., Lannuzel, D., Remenyi, T., Sarthou, G., Aumont, O., Gehlen, M., and Jeandel, C.: Hydrothermal contribution to the oceanic dissolved iron inventory, Nat. Geosci., 3, 252–256, doi:10.1038/NGEO818, 2010. 14546
Talley, L., Reid, J., and Robbins, P.: Data-based meridional overturning streamfunctions for the global ocean, J. Climate, 16, 3213–3226, doi:10.1175/1520-0442(2003)016<3213:DMOSFT>2.0.CO;2, 2003. 14551
Textor, C., Schulz, M., Guibert, S., Kinne, S., Balkanski, Y., Bauer, S., Berntsen, T., Berglen, T., Boucher, O., Chin, M., Dentener, F., Diehl, T., Easter, R., Feichter, H., Fillmore, D., Ghan, S., Ginoux, P., Gong, S., Grini, A., Hendricks, J., Horowitz, L., Huang, P., Isaksen, I., Iversen, I., Kloster, S., Koch, D., Kirkevåg, A., Kristjansson, J. E., Krol, M., Lauer, A., Lamarque, J. F., Liu, X., Montanaro, V., Myhre, G., Penner, J., Pitari, G., Reddy, S., Seland, Ø., Stier, P., Takemura, T., and Tie, X.: Analysis and quantification of the diversities of aerosol life cycles within AeroCom, Atmos. Chem. Phys., 6, 1777–1813, doi:10.5194/acp-6-1777-2006, 2006. 14547
Thorstenson, D. and Plummer, L.: Equilibrium criteria for two-component solids reacting with fixed composition in an aqueous phase; example, the magnesian calcites, Am. J. Sci., 277, 1203–1223, doi:10.2475/ajs.277.9.1203, 1977. 14565, 14566
Tréguer, P. and De La Rocha, C.: The World Ocean Silica Cycle, Annu. Rev. Mar. Sci., 5, 477–501, doi:10.1146/annurev-marine-121211-172346, 2013. 14542

BGD
10, 14539–14593, 2013

van Bennekom, A., Buma, A., and Nolting, R.: Dissolved aluminium in the Weddell-Scotia Confluence and effect of Al on the dissolution kinetics of biogenic silica, Mar. Chem., 35, 423–434, doi:10.1016/S0304-4203(09)90034-2, 1991. 14543

van Beusekom, J. and Weber, A.: Decreasing diatom abundance in the North Sea: the possible significance of aluminium, Olsen Int. S., 121–127, 1992. 14543

van Hulten, M. M. P., Sterl, A., Tagliabue, A., Dutay, J.-C., Gehlen, M., de Baar, H., and Middag, R.: Aluminium in an ocean general circulation model compared with the West Atlantic Geotraces cruises, J. Marine Syst., doi:10.1016/j.jmarsys.2012.05.005, 2012. 14542, 14543, 14544, 14545, 14547, 14580

Vink, S. and Measures, C.: The role of dust deposition in determining surface water distributions of Al and Fe in the South West Atlantic, Deep-Sea Res. Pt. II, 48, 2787–2809, doi:10.1016/S0967-0645(01)00018-2, 2001. 14579

Wedepohl, K.: The composition of the continental crust, Geochim. Cosmochim. Ac., 59, 1217–1232, doi:10.1016/0016-7037(95)00038-2, 1995. 14547

BGD
10, 14539–14593, 2013

Table 1. Parameters for the reference simulation.

Parameter	Symbol	Value
mass fraction of Al in dust	f_{Al}	8.1 %
surface dissolution fraction	α	5 %
partition coefficient	k_d	4×10^6 dm^3 kg^{-1}
first order rate constant	κ	10^4 yr^{-1}
settling speed of Al_{part}	w_s	30–200 m d^{-1}

BGD
10, 14539–14593, 2013

Table 2. Overview of the reference and sensitivity experiments.

Experiment	sediment	incorporation
Reference experiment	no	no
Sediment resuspension	independent of $[Si_{diss}]$	no
Sediment resuspension	depends on bottom $[Si_{diss}]$	no
Incorporation	no	yes
Incorporation + lower k_d	no	yes

BGD
10, 14539–14593, 2013

Table 3. Observational data used for comparison with model. For positions see Fig. 3.

Cruise	Ocean	Source	#
ARK XXII/2	Arctic	Middag et al. (2009)	1080
ANT XXIV/3	Southern	Middag et al. (2011b)	919
SAZ-Sense	Southern	Remenyi (2013)	146
SR3	Southern	Remenyi (2013)	292
64 PE 267	Atlantic	Middag et al. (2013b)	137
64 PE 319	Atlantic	Middag et al. (2013b)	383
64 PE 321	Atlantic	Middag et al. (2013b)	504
64 PE 538	Atlantic	Middag et al. (2013b)	120
JC057	Atlantic	Middag et al. (2013b)	432
Subtotal used primarily for detailed comparison			4013
IOC96	Atlantic	Vink and Measures (2001)	1048
M 60	Atlantic	Kremling (1985)	91
IRONAGES III	Atlantic	Kramer et al. (2004)	181
EUCFe	Pacific	Slemons et al. (2010)	195
MC-80	Pacific	Orians and Bruland (1986)	92
VERTEX-4	Pacific	Orians and Bruland (1986)	54
VERTEX-5	Pacific	Orians and Bruland (1986)	59
KH-98-3	Indian	Obata et al. (2007)	152
Subtotal of other observations for global comparison			1872
Grand total of all dissolved Al values			5885

BGD
10, 14539–14593, 2013

Table 4. Statistics of [Si_{diss}] (first two rows) and [Al_{diss}] (other rows) of the simulations, in the West Atlantic Geotraces section.

Experiment	RMSD	RMSD$_{\updownarrow}$	significance$_{\updownarrow}$	2σ range$_{\updownarrow}$	r	RI	RI$_{\updownarrow}$
[Si_{diss}]							
van Hulten et al. (2012)	23.9 µM	39.8 µM	–	[35.1, 44.4]	0.938	3.70	2.42
Reference experiment	12.4 µM	18.0 µM	improvement	[15.8, 20.2]	0.769	3.70	1.93
[Al_{diss}]							
van Hulten et al. (2012)	7.13 nM	8.24 nM	–	[7.34, 9.11]	0.545	1.94	1.90
Reference experiment	7.53 nM	7.65 nM	insignificant	[6.82, 8.44]	0.478	1.92	1.78
Reference experiment	7.53 nM	7.65 nM	–	[6.82, 8.44]	0.478	1.92	1.78
Resuspension everywhere	6.76 nM	5.06 nM	improvement	[4.70, 5.42]	0.505	1.90	1.63
Resusp depend [Si_{diss}]	6.67 nM	4.71 nM	improvement	[4.40, 5.01]	0.517	1.94	1.59
Incorporation	12.84 nM	9.85 nM	worsening	[9.03, 10.65]	0.221	3.21	2.42
Incorporation + lower k_d	11.59 nM	8.68 nM	worsening	[7.95, 9.40]	0.229	2.28	1.94

BGD
10, 14539–14593, 2013

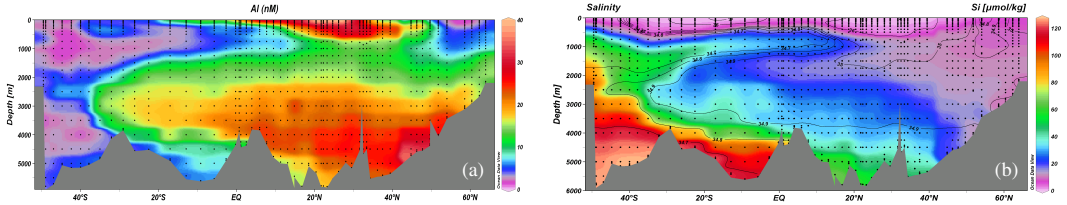

Fig. 1. Observations of **(a)** [Al_{diss}] (nM) and **(b)** [Si_{diss}] (µM) at the West Atlantic Geotraces section (Middag et al., 2013b).

BGD
10, 14539–14593, 2013

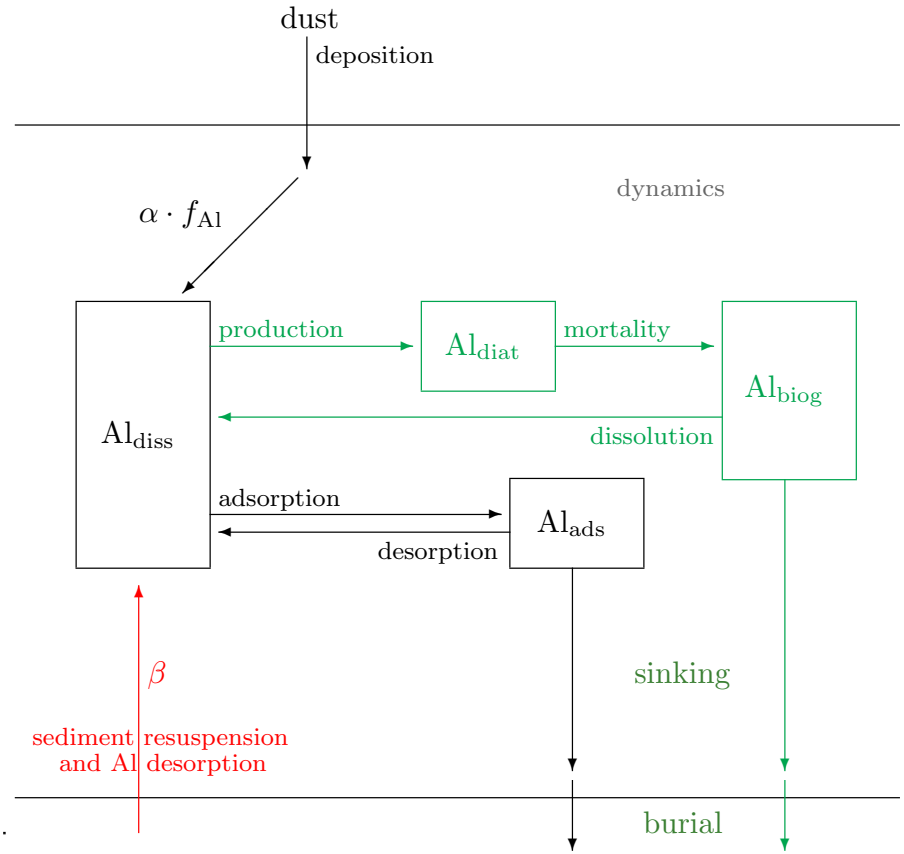

Fig. 2. Model scheme. Here $f_{Al} = 8\%$ is the fraction of Al in dust and $\alpha = 5\%$ is the fraction dissolving in the surface ocean. Reference model in black; sediment resuspension and subsequent Al dissolution in red; biological incorporation and subsequent mortality and dissolution in green. For Si there are three similar pools Si_{diss}, Si_{diat}, Si_{biog} but no adsorbed pool. Furthermore, the biological and sinking processes (green arrows) also apply for these Si pools.

BGD
10, 14539–14593, 2013

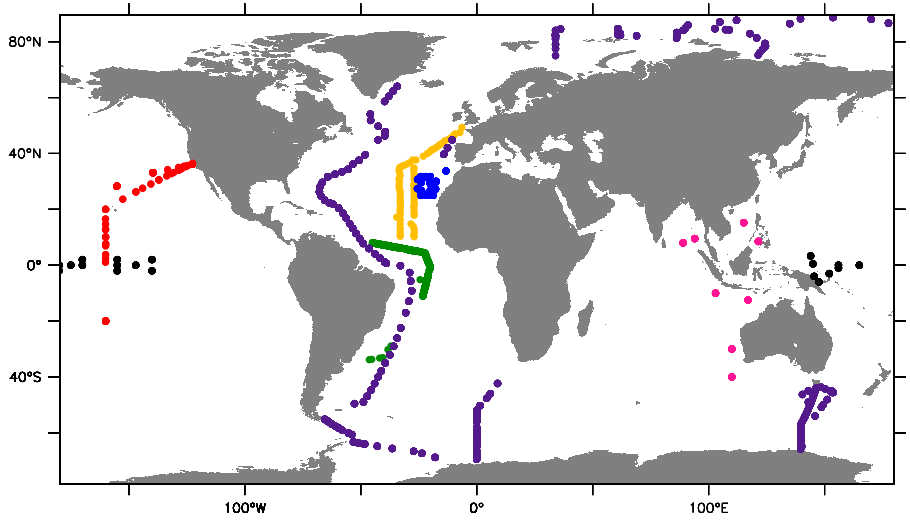

Fig. 3. Stations of the cruises: M 60 (yellow); MC-80 and VERTEX (red); IOC96 (green); IRONAGES III (blue); KH-98-3 (pink); EUCFe (black); Geotraces (purple). See Table 3 for an overview with references and the number of observations.

BGD
10, 14539–14593, 2013

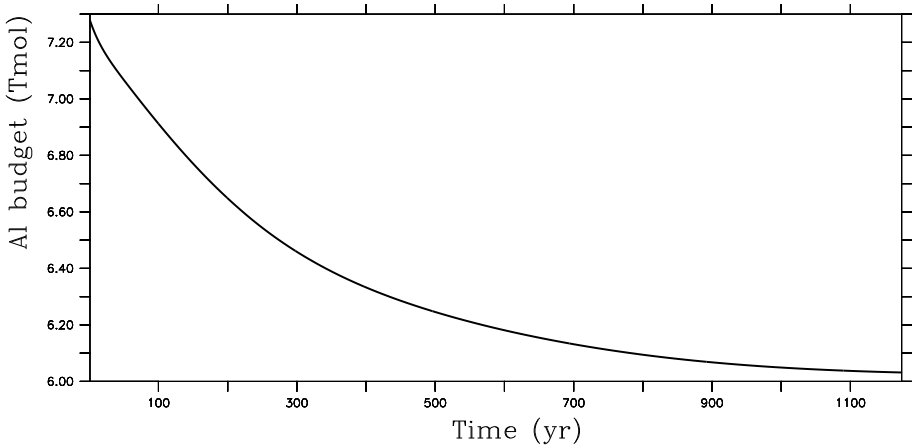

Fig. 4. Total Al budget $[Al_{ads}] + [Al_{diss}]$ (Tmol) for the reference simulation in the world ocean, as a function of time (model years).

BGD
10, 14539–14593, 2013

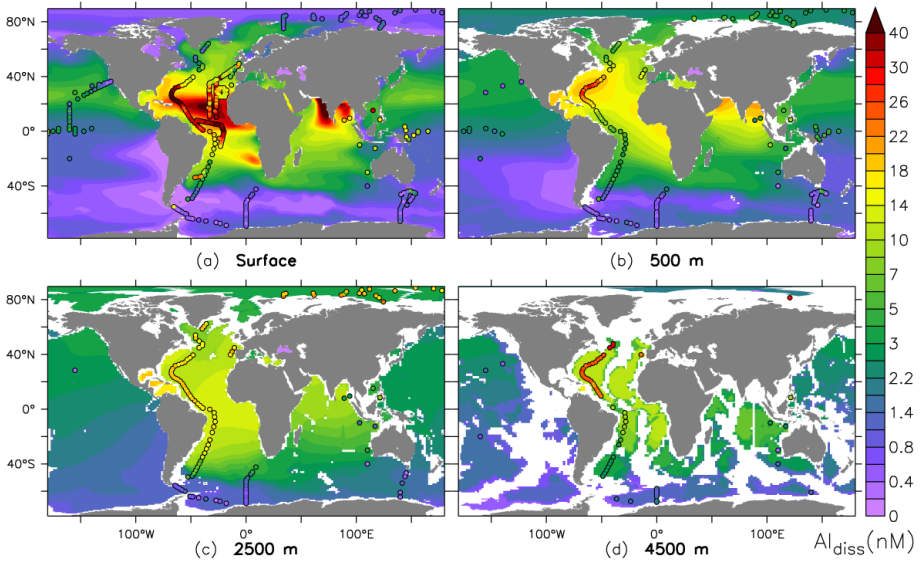

Fig. 5. Average of the final model year (1250) of the dissolved aluminium concentration (nM) from the reference experiment at four depths.

BGD
10, 14539–14593, 2013

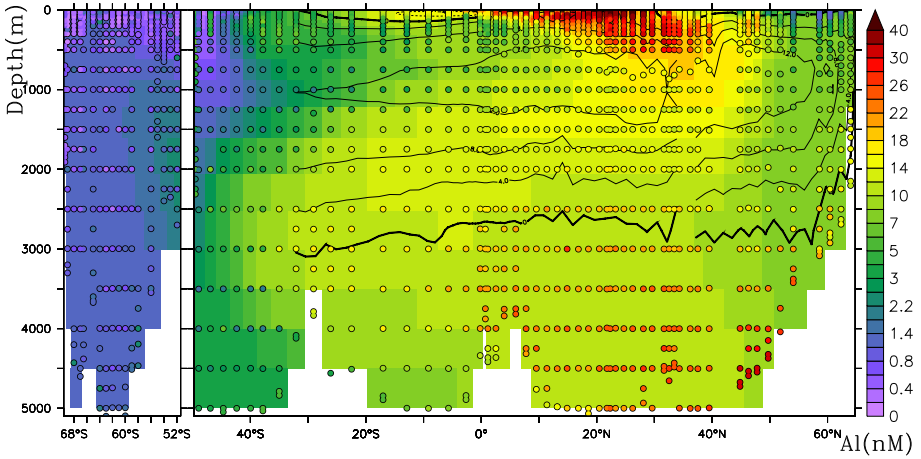

Fig. 6. Dissolved aluminium (nM) from the reference experiment (year 1250) along the Zero Meridian and West Atlantic Geotraces section. Observations are presented as coloured dots. The contour is the Atlantic Overturning Stream Function (OSF), only defined north of Cape Agulhas and away from 36° N where cross-land mixing through the unresolved Strait of Gibraltar does not allow for a well-defined OSF.

BGD
10, 14539–14593, 2013

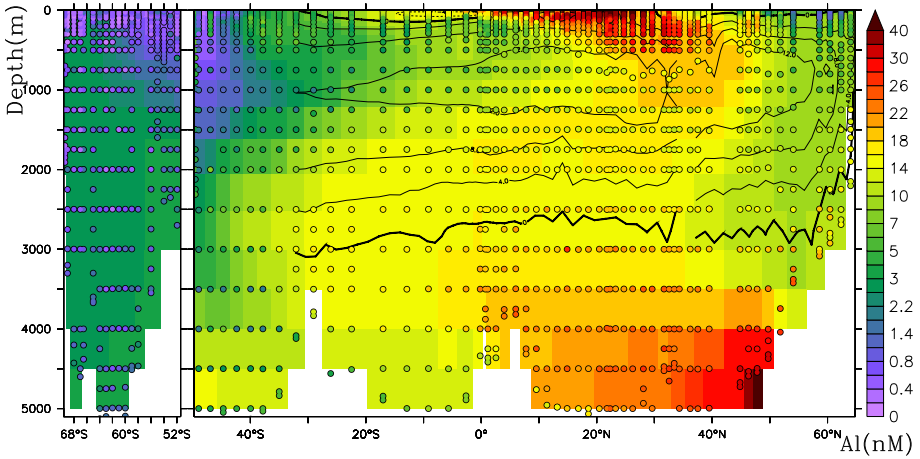

Fig. 7. Simulated [Al_{diss}] (nM) from the [Si_{diss}] independent sediment resuspension experiment (250 yr after forking) along the Zero Meridian and West Atlantic Geotraces section. Observations are represented by the coloured dots.

BGD
10, 14539–14593, 2013

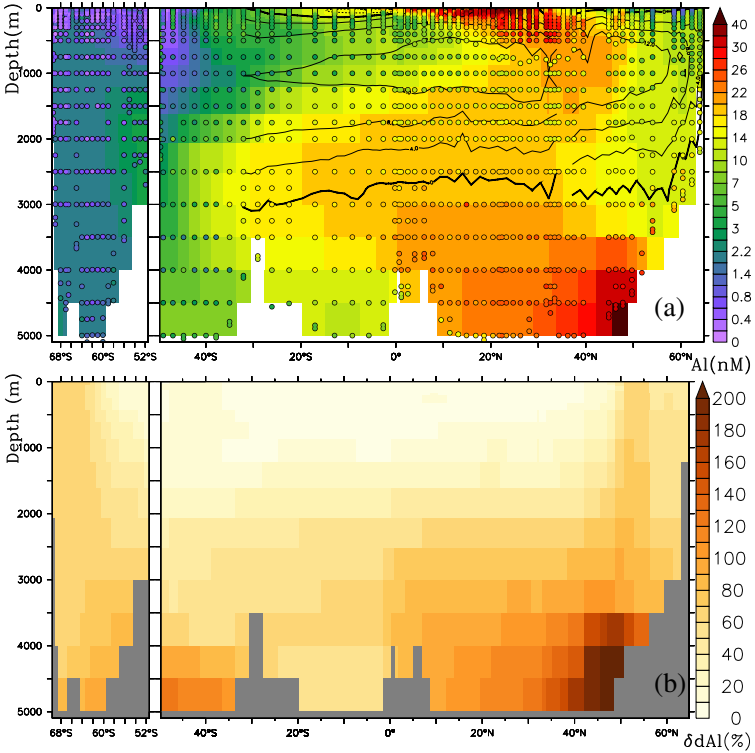

Fig. 8. Results from the [Si_{diss}]-dependent sediment resuspension experiment (250 yr after forking) along the Zero Meridian and West Atlantic Geotraces sections. **(a)** Modelled [Al_{diss}] (nM) with observations plotted as coloured dots. **(b)** Relative difference (%) with the reference simulation.

BGD
10, 14539–14593, 2013

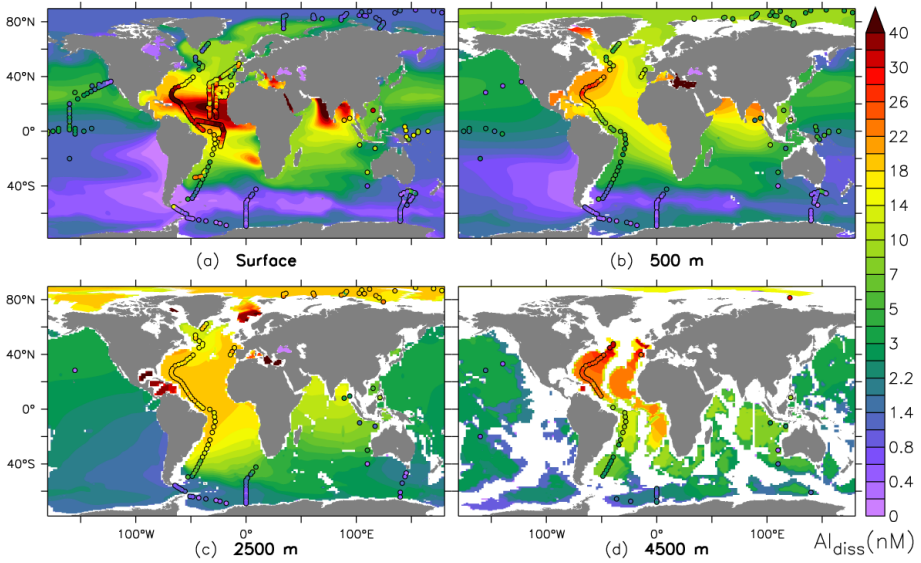

Fig. 9. [Al_{diss}] (nM) of the [Si_{diss}]-dependent simulation with sediment resuspension at four depths (250 yr after forking).

BGD
10, 14539–14593, 2013

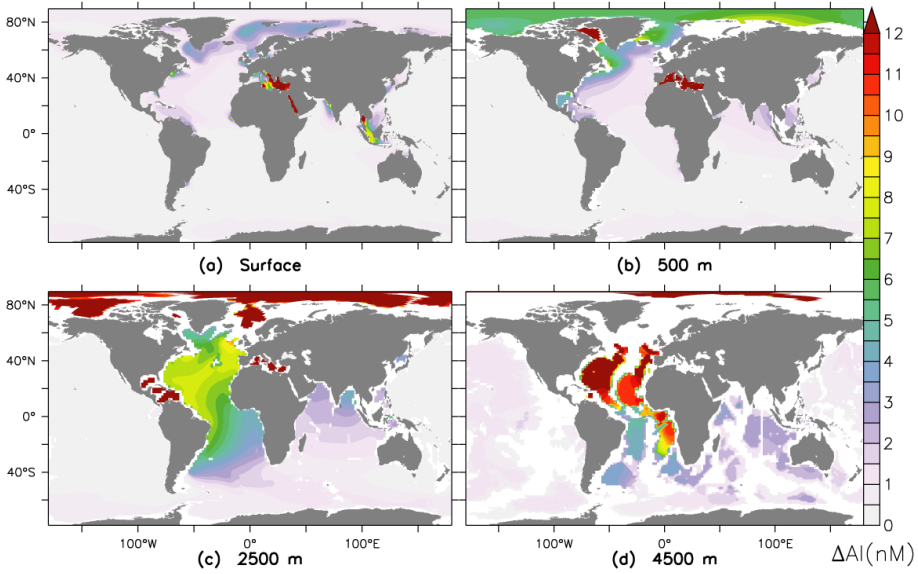

Fig. 10. Difference of [Al_{diss}] (nM) between the run with [Si_{diss}]-dependent sediment resuspension and the reference run at four depths (250 yr after forking).

BGD
10, 14539–14593, 2013

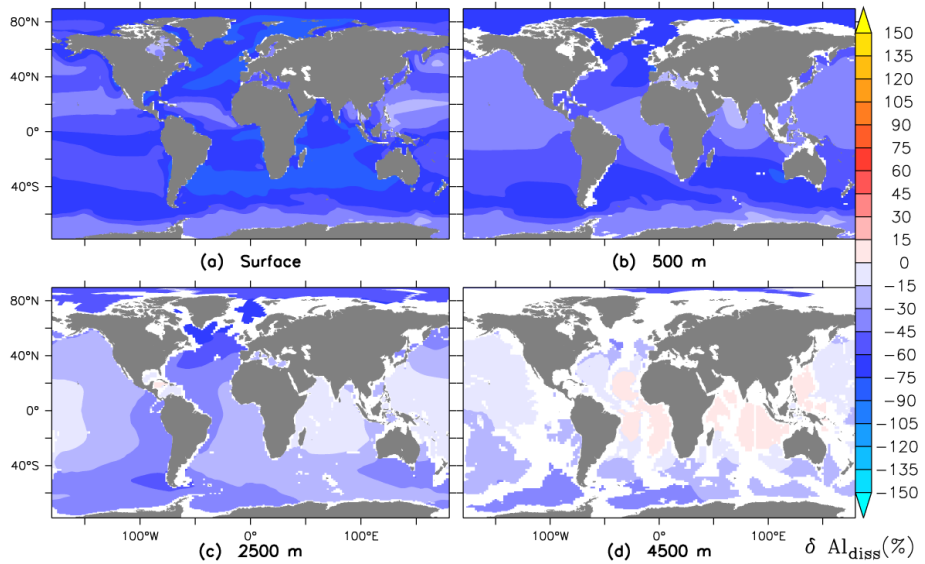

Fig. 11. Relative difference of [Al_{diss}] (%) between the run with biological incorporation and the reference run at four ocean depths (average over year 200).

BGD
10, 14539–14593, 2013

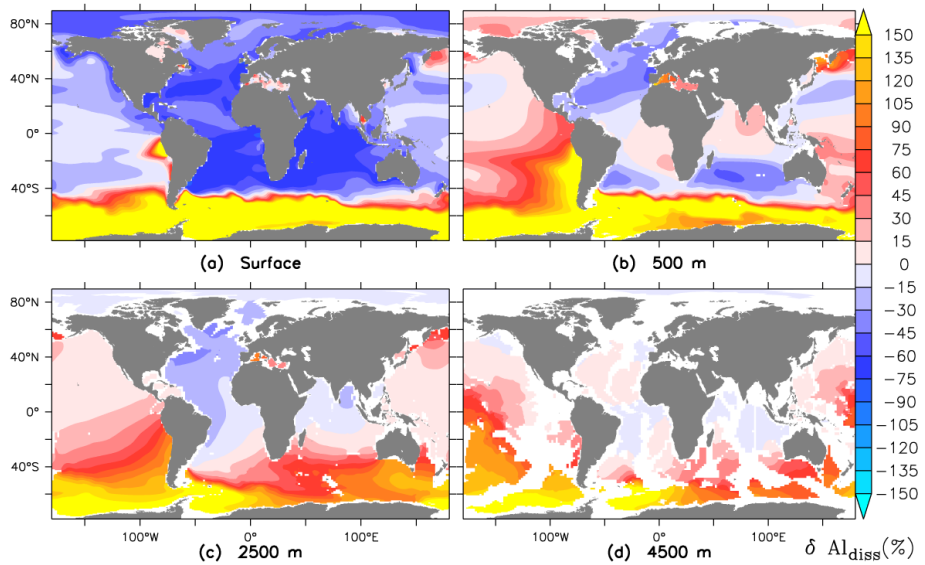

Fig. 12. Result of a 200 yr simulation with incorporation (no limitation, i.e. $\xi = [Al_{diss}]/[Si_{diss}]$) and a decreased scavenging partition coefficient $k'_d = k_d/4 = 1 \cdot 10^6\,dm^3\,kg^{-1}$. Relative difference of $[Al_{diss}]$ between this simulation and the reference simulation (average of final year).

BGD
10, 14539–14593, 2013

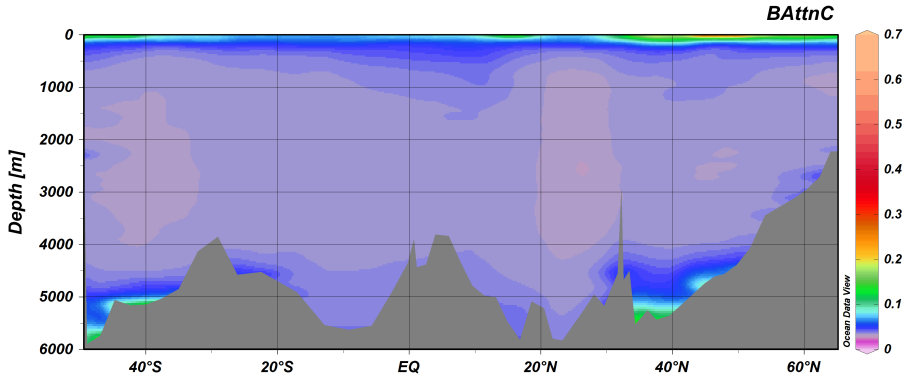

Fig. A1. Beam attenuation coefficient, a measure of the amount of particles (e.g. Behrenfeld et al., 2006). Courtesy of Micha Rijkenberg.

BGD
10, 14539–14593, 2013